DISCLAIMER NOTICE

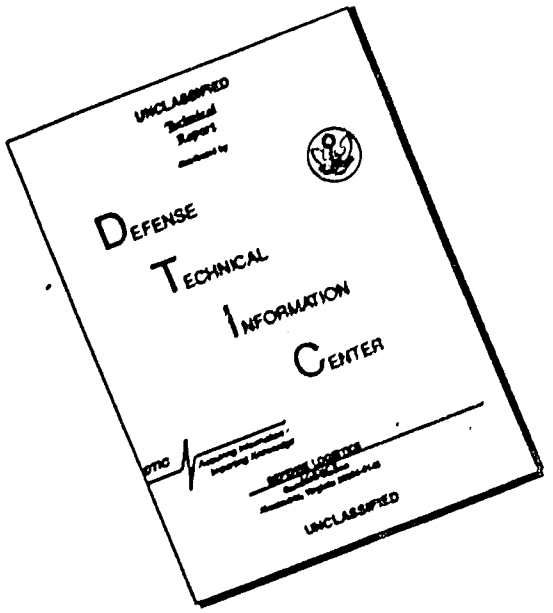

THIS DOCUMENT IS BEST QUALITY AVAILABLE. THE COPY FURNISHED TO DTIC CONTAINED A SIGNIFICANT NUMBER OF PAGES WHICH DO NOT REPRODUCE LEGIBLY.

El Grupo Solar Radar Antenna

M. H. Dwinell
A. R. Dion

Technical Report No. 276

27 August 1962

Lincoln Laboratory
MASSACHUSETTS INSTITUTE OF TECHNOLOGY

MASSACHUSETTS INSTITUTE OF TECHNOLOGY

LINCOLN LABORATORY

THE EL CAMPO SOLAR RADAR ANTENNA

M. E. DEVANE

A. R. DION

Group 315

TECHNICAL REPORT NO. 276

17 AUGUST 1962

ABSTRACT

An antenna is described for use in a radar system designed to study reflections of VHF electromagnetic waves from the sun. This antenna consists of two rectangular planar arrays which occupy the same land surface and have dipole elements that are mutually perpendicular. The elements are excited by a combination of parallel and series feed networks. Each array produces a 0.75° by 12° fan-shaped beam whose direction is set by the adjustment of the phase of the element currents. So far, the beam has been confined to directions located in the north-south plane which range from near broadside to 52.5° south from broadside. Good performance for these beam directions was obtained with only two settings of the element-matching network.

The directivity patterns of one of these arrays were measured by flying a properly instrumented airplane in its Fresnel region and good agreement with theoretical predictions was obtained.

LEXINGTON MASSACHUSETTS

THE EL CAMPO SOLAR RADAR ANTENNA

I. INTRODUCTION

The possibility of radar observations of the sun has been considered for over a decade.[1] Lincoln Laboratory has recently obtained satisfactory radar returns at its remote site near El Campo, Texas.[2] The radar system consists of a 520-kw CW transmitter, a planar array of dipoles and suitable receiving and detecting equipment. This report describes the antenna design, its performance and some of the salient difficulties encountered during its installation and initial operating periods.

A study of several antenna configurations, together with their construction and maintenance costs, led to the conclusion that observations could best be made by allowing the sun to drift through the antenna beam. Also, system requirements and cost considerations fixed the antenna gain at about 33 db. With uniform illumination and an assumed efficiency of 55 percent, the corresponding beamwidth product is about $(1)^2$. In order that the gain variation during the transmission period be small, it is necessary to make the E-W (east-west) beamwidth appreciably larger than the amount of earth rotation during this period. The transmission period lasts about 10 minutes, which is the duration of the round trip to the sun, and during this time the earth rotates 4°. On the other hand, a large value of the E-W beamwidth implies a small N-S (north-south) beamwidth which requires a long antenna, and therefore a larger feed network loss. These characteristics resulted in the choice of a beam 0.75° × 12° wide at broadside. Since the midday sun declination at the site varies during the year, between 5.5° and 52.5° south, the "fan-shaped" beam must be capable of being scanned at least over this range. In view of the desired radiation properties, an antenna was chosen which was made up of an array of dipoles excited by a feed system. This system could be modified on a day-to-day basis, so that the beam axis would point toward the average position of the sun during the time it would pass through the beam. In order to derive maximum information, signals were transmitted linearly polarized in a given direction and were received polarized in both the given and the orthogonal directions. Two array antennas, cross-polarized with respect to one another, are used for this purpose. The first, referred to as the principal antenna, is used for transmitting and receiving signals polarized in the E-W direction, and is described in Sec. II. The second, or the orthogonal, antenna is used for receiving signals polarized in the N-S direction and is the subject of Sec. III.

II. PRINCIPAL ARRAY ANTENNA

The principal array antenna was designed to meet the following specifications:

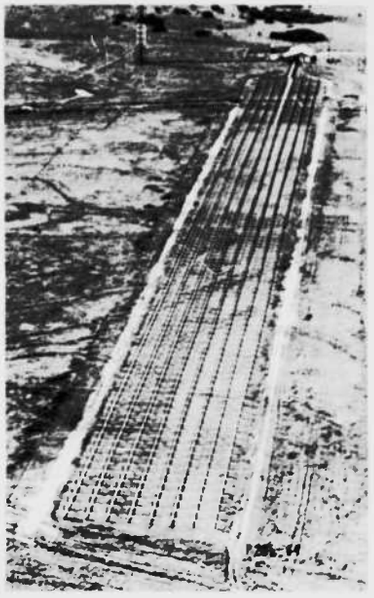

(a) Aeriol view.

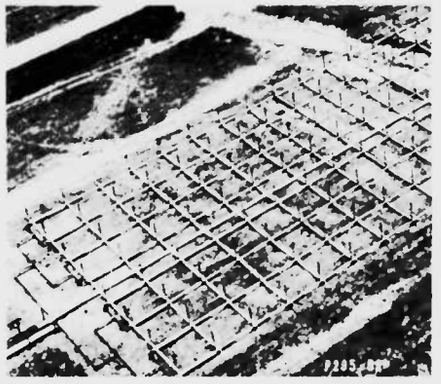

(b) Feed end.

Fig. 1. El Campo array.

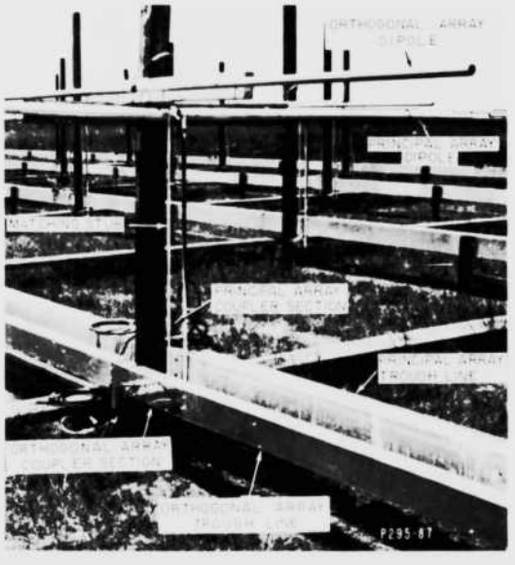

Fig. 2. Photograph of one element of the principal and the orthogonal arrays.

Beamwidth of broadside beam	$12^\circ \times 0.75^\circ$
Input power	600 kw
Input VSWR	1.20:1.00
Operating frequency	38.25 Mcps
Polarization	Linear, parallel to the ground and oriented E-W
Gain	Maximum possible consistent with the other requirements
Beam direction	Manually adjusted to any direction located within a 120° cone* centered on the zenith direction

In addition, the radiation patterns should be free of a grating lobe for all the beam directions specified above.* The most important characteristic of the antenna is its gain, which should be maximized by a low-loss feed network and a uniform excitation of the elements. To be consistent with costs, the total attenuation of the feed network was specified as less than 2 db.

The general design of the principal array antenna was carried out by members of Lincoln Laboratory. Completion of the design and construction of the array was the responsibility of Radiation Engineering Laboratory (Maynard, Massachusetts).

A. General Description

In order to form the $0.75^\circ \times 12^\circ$ broadside beam, a uniformly illuminated aperture of 67.2 × 4.2 wavelengths square (1730 × 108 feet) is required. This factor and the scanning requirement necessitate the use of an array. The grating lobe specification was satisfied by disposing the elements on a square lattice 0.534λ (13.75 feet) on the side. A total of 1024 elements was used in a 128-column × 8-row matrix (Fig. 1(a-b)). The array is mounted over a level ground and therefore its broadside direction is toward zenith. The peak directivity of an aperture of equal area is 55.6 db for the broadside beam. Each element is a center-fed near-half-wave dipole mounted parallel to ground, 4-3/4 feet above it (Fig. 2), and polarized in the E-W direction. Shunted across the feed point is a short-circuited section of a two-wire transmission line. Its length and the length of the dipole are so chosen that the feed point impedance is about 112 ohms. (This particular choice of matching network was chosen for reasons which will become apparent in Sec. II-B-7-a.) A 75-ohm transmission line, one-quarter wavelength long, transforms this impedance to a driving point value of about 50 ohms.

The transmitter has two 6-1/8 inch coaxial transmission line output terminals from which 520 kw of average power is available. The power from each of these lines is divided into four equal amounts to excite the eight main feeder lines of the array.

The feeder lines are a unique design of "trough" lines; they comprise a center conductor which is a continuation of the inner conductor of the 6-1/8 inch transmission line and an outer conductor similar to an aluminum channel, or trough. The use of this type of line instead of standard coaxial transmission lines of equivalent electrical characteristics reduced the cost of the antenna approximately 25 percent.

At each element (every 13-3/4 feet along the feeder lines) there is a device (coupler) which extracts some of the energy from the main line. These couplers are adjusted so that each element radiates approximately the same amount of power.

* The solid angle covered by this specification is substantially larger than that required for sun studies only. The desire to make the antenna suitable for other radio astronomy studies justifies the increase.

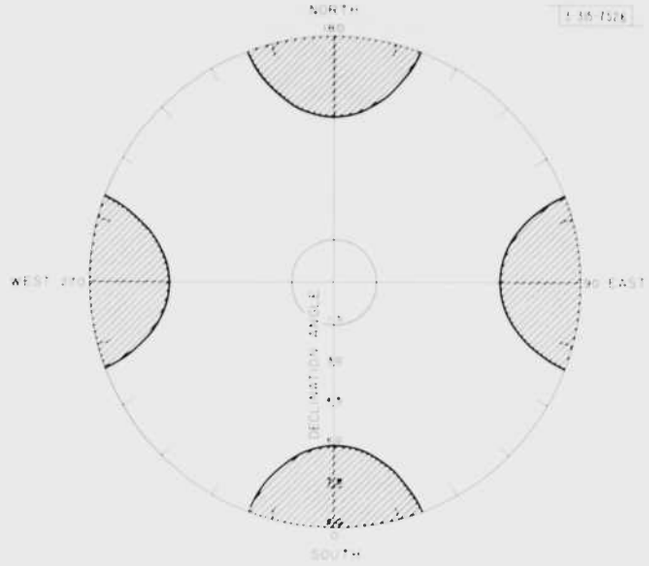

Fig. 3. Solid angle over which the beam of the principal array antenna can be scanned without the formation of a grating lobe (outside shaded area).

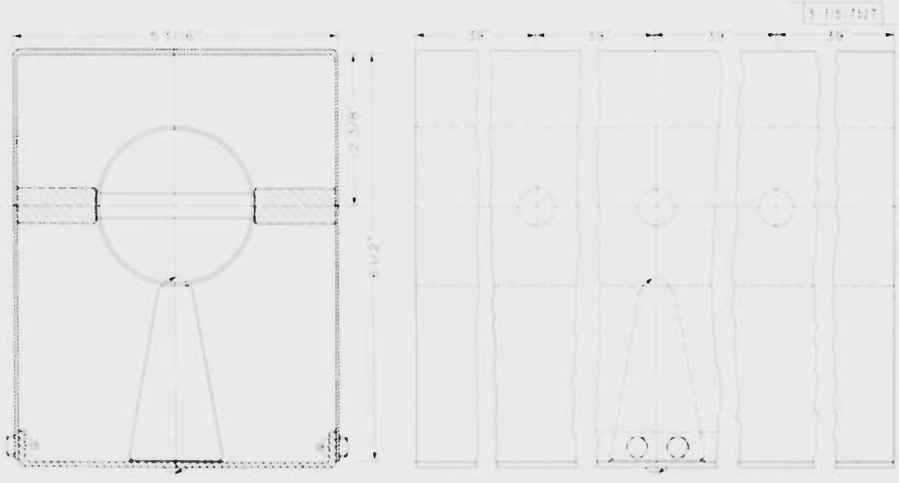

Fig. 4. Geometry of trough line.

In order to scan the beam, the phase of the current in each element must be capable of being changed. This phase is adjusted by inserting the proper length of 50-ohm (RG-8/U) cable between the couplers and the driving point of the elements. The required cable length is obtained by the combination of four cables with the lengths $\lambda_c/2$, $\lambda_c/4$, $\lambda_c/8$, and $\lambda_c/16$ (λ_c is the wavelength in the cable). The phase of the exciting current of each element may thus be adjusted to within 11.25° of the desired value.

B. Detailed Description

1. Element Spacing

In order to realize the array with a minimum number of elements, the spacing between elements must be as large as feasible without deteriorating the radiation pattern by the appearance of a grating lobe. This requirement establishes the maximum spacing between elements for a given lattice arrangement and for a given maximum scan angle. A square-lattice arrangement was chosen for the transmitting array. A triangular lattice would have been a better choice because a reduction of about 13 percent of the number of elements needed would have resulted.[3] However, this fact became known to the authors too late. For the square lattice, the maximum spacing d_{max} between elements is obtained from the relation

$$d_{max} = \lambda/(1 + \sin\theta_{max}) \quad , \tag{1}$$

where θ_{max} is the largest scan angle, measured from the array normal. For $\theta_{max} = 60°$, $d_{max} = 0.5359\lambda$. A design value of 0.5343λ (13 feet 9 inches at the design frequency) has been chosen. With this spacing, the pattern is free of a grating lobe for scan angles as large as 60.67° in the two principal planes. In other planes, this property exists for still larger scan angles, as shown in Fig. 3. (In this figure, radial distances are proportional to declination angles, and azimuth is measured from the south.) The scan angles for which a grating lobe exists are located in the shaded regions of the figure. The boundary between the two regions is the locus of beam directions for which a grating lobe is formed in the plane of the array. The amplitude of this lobe is very small because the elements radiate very little energy in, or near, this plane.

2. Feed Network

a. Feeder Lines

The 520-kw output of the transmitter is supplied in two 6-1/8 inch coaxial lines. Each of these outputs is divided into four equal parts by three 2:1 power dividers which consist of a standard 6-1/8 inch tee and a quarter-wavelength transformer to convert the 25-ohm impedance level at the center of the tee to the 50-ohm characteristic impedance of the transmission line. Eight transitions connect the eight 6-1/8 inch coaxial lines to the trough lines. The geometry of the trough line is shown in Fig. 4. Its center conductor is a continuation of the center conductor of the 6-1/8 inch line (2.500-inch-diameter copper tubing). The outer conductor is an alclad aluminum sheet bent in a channel, or trough; the copper-center conductor was used to reduce the transmission line loss. The characteristic impedance of this particular line is adjusted by the proper selection of the distance of the center conductor from the top of the trough. The position indicated in Fig. 4, with the center of the inner conductor 2-3/8 inches from the top inside surface, results in a 50-ohm characteristic impedance.

The inner conductor is centered side-to-side by steatite insulators spaced approximately 4 feet apart. The top-to-bottom ratio is maintained by attaching the inner conductor to a conical-shaped insulator which is then fastened to straps across the bottom of the trough. The small eccentricities which can still occur cannot affect the characteristic impedance substantially.

Every 13-3/4 feet (at each coupler) the inner conductor is changed to a 2.600-inch OD conductor for a 4-inch length. This permits the 2.5-inch inner conductor to slip inside this latter (Fig. 5) and the two are pulled together by a hose-type clamp to insure good contact. This arrangement also permits the disassembly of each coupler individually. The outer conductor at the coupler location is a casting 9 inches long.

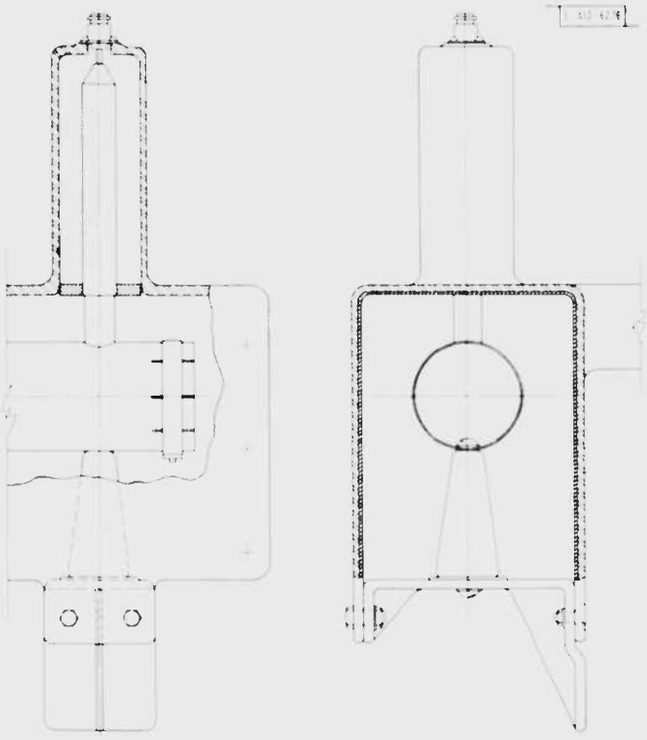

Fig. 5. Coupler section.

With a trough-transmission line, a small amount of power is radiated through the open side. If the combination of conductor loss and radiated loss is equal to, or less than, the transmission loss of the standard 3-1/8 inch coaxial transmission line, which was considered to have satisfactory performance, the trough line will also be satisfactory. Since the loss of 3-1/8 inch line is 0.0007 db/foot at the operating frequency, the usual methods of measuring insertion loss cannot be used. Therefore, an open-circuited half-wavelength section of trough line and of 3-1/8 inch coaxial line, both of which had adjustable inner conductor lengths, was constructed and the transmission loss was determined by the cavity-resonance method.[4] Resonance is obtained by changing either the length of the inner conductor L or the frequency f. The attenuation constant α of the transmission line is related to the measured Q, at resonance, by the formula

$$\alpha = \frac{\pi}{Q\lambda}$$

and Q is given by

$$Q = \frac{L_o}{2\Delta L} = \frac{f_o}{2\Delta f} ,$$

where ΔL or Δf is the change in L_o or f_o, respectively, which results in a 3.0-db reduction in the response of the cavity compared with the response obtained at resonance. The quantity L_o is the resonant length and f_o is the resonant frequency. The measurements were carried out at 39 Mcps. The measured Q for the 5-1/8 inch line was 1300, whereas that of the trough line was 1745. The loss of this latter is therefore approximately two-thirds that of the 5-1/8 inch line. Based on these results, the estimated loss for the 1750-foot trough line is 1.1 db at 38.39 Mcps.

Two 1750-foot lengths of the trough line were installed with the open side about one foot above the ground. A series of electrical measurements was begun. After a period of time, we observed that the insertion loss of the feeder lines changed from day to day, and under certain conditions it was as large as 10 db. At first we assumed that the excess loss was caused by insects (spiders and mud daubers) which had invaded the line and made nests. However, cleaning out these nests did not substantially decrease the loss. Furthermore, the high loss was measured after a rain storm when the ground was very wet. To check the effect of the wet ground, the Q measurement was repeated with the open side of the resonant length of trough line resting on some mud. In this condition, the loss increased by only a small quantity which corresponded to a total attenuation of approximately 2 db for the 1750-foot length. When the trough line was positioned slightly above the ground, no increase in the loss was noticed.

Next, the bottom of a 1750-foot length of the trough line was covered with aluminum foil; this reduced the measured attenuation to less than 1.5 db. Since the energy radiated from the open side could account for only a very small part of the excessive loss, further experiments were conducted which indicated that the increase in insertion loss was due to the grass growing close to the trough lines. The grass was cut and eliminated from the area immediately under the trough line opening by placing roofing paper over it. In addition to this, a grass-growth retarder was sprayed over the entire area below the antenna array. The remaining trough lines were installed in the same manner and the measured attenuation was approximately 1.25 db. On occasion, the attenuation of a given line has increased to approximately 2 db, this is probably due to moisture accumulation on the wood supports.

b. Couplers

Power from the series feed lines is diverted to the branch lines by the capacitive couplers. The amount of coupling is determined, among other factors, by the required distribution of power among the elements. Calculation of the coupling value as a function of coupler location along the line has been carried out for a uniform distribution of this power and is the subject of the next section. When the calculated coupling values are approximate to ±0.5 db, the realization of a feeder line requires couplers of 16 different coupling values.

The physical characteristics of the couplers designed by Radiation Engineering are illustrated in Fig. 6. A cylindrical condenser in series with the center conductor of the branch line controls coupling. All couplers have the same dimensions, except for the length of the condenser center electrode which is adjusted to yield the required coupling. The 1/16-inch electrode gap is maintained by means of a polyethylene tube. These couplers failed to meet the power requirement (125 kw), and broke down at much smaller power levels. Fortunately this fault was corrected

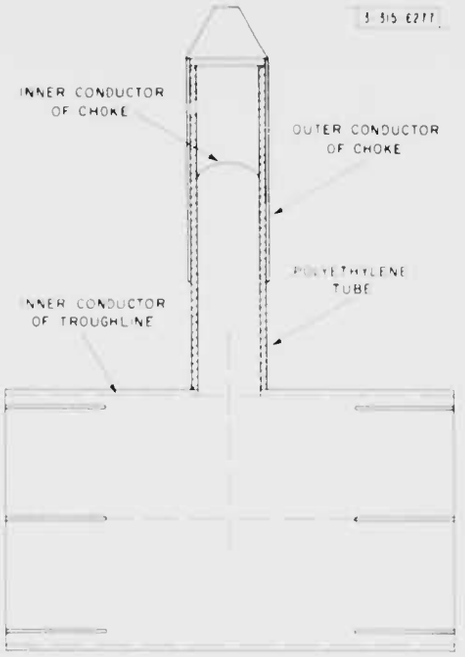

Fig. 6. Coupler design.

with only minor modifications. However, these modifications delayed the antenna's completion because construction of the feeder lines with the defective couplers had already been completed when the coupler deficiency was found.

It is interesting to review some of the factors which led to the failure of the couplers, and to point out the main features of the modified versions, together with their degree of success. All eight feeder lines, which used couplers of the original design (Fig. 6), were tested successfully with 15,000 volts DC applied between the inner and outer conductors of the trough lines. However, when RF power was applied to two of the feeder lines, breakdown occurred with an input power less than 50 kw/line, corresponding to a maximum potential difference across the condensers of less than 1200 volts rms. (The exact breakdown power level is not known because these tests were carried out by firing the radar transmitter into only two feeder lines, and this transmitter had no provision for operation at power levels less than 50 kw/line.) The wide spread between the measured value of the DC and the RF tests is indicative that the AC breakdown was brought about through the action of an overlooked physical phenomenon. This phenomenon is believed to be the low-current density discharge that may take place under certain conditions at radio frequencies. Because of the alternating nature of the current, this discharge does not require a supply of electrons from the electrodes (as opposed to a DC discharge). Consequently this discharge can exist even though a solid dielectric is interposed between the electrodes, provided a suitable air gap is left in which the electric field exceeds the air breakdown potential. The heat generated by this low-current density discharge may cause progressive softening and melting of the dielectric material, or a progressive carbonization of its surface, both cases eventually leading to the formation of an arc between the electrodes. This breakdown mechanism was likely to happen in the original coupler design, air gaps existed along the electric path lines at both the base and top of the capacitor, and could also have existed in the intervening region as a result of tolerance combinations. It can be verified that the electric field in this last region exceeds air breakdown potential (about 40,000 volts/inch at RF) when the coupler is subjected to an input

power of 20 kw only. The breakdown potential at the base, where a sharp corner exists, is exceeded with even lower input power levels.

It is obvious that the use of a dielectric tubular spacer, instead of increasing the breakdown potential (as is the case for DC), contributes to its decrease at RF, because the electric field in the remaining small air gaps is raised by a factor nearly equal to the dielectric constant. It is also obvious that one way to improve the breakdown characteristics of the couplers is to fill in all air gaps where the electric field exceeds air breakdown potential, with a dielectric of better breakdown characteristics. This was accomplished by means of a dielectric grease (Dow Corning No. 4) with the anticipated results. However, this solution was not suitable for a long period of time, since a slight discoloration of the grease was observed after a short time. This behavior, coupled with the difficulties experienced in trying to eliminate all air pockets in the capacitors, made it necessary to reject this corrective method. Another solution which had partial success is indicated in Fig. 7. This design is characterized by larger electrode spacing and by the absence of solid dielectrics in most regions of high electric field. Tests performed on seven couplers of different coupling values showed their breakdown to occur somewhere near 150 kw (between two to five times the maximum operating power). However, when the required coupler modifications were incorporated in most of the feeder-line couplers (they were incorporated on the first 105 couplers of all eight feeder lines only, since the power level on the remaining ones was below their estimated breakdown value) and high-power testing of the feeder lines was resumed, an appreciable number still failed at powers below the maximum operating levels. When the defective couplers were replaced, it was possible to operate the lines at full power and to use the system for radar observations of the sun, but failures still occurred in a sporadic manner and resulted in the abortion of many experiments. The failures then occurred at the top spacer of the capacitors and it was conjectured that, in order to obtain a performance comparable to that of the test models, close tolerances on the manufacture and assembly of this spacer were required principally on the amount of pressure exerted by the supporting screw. It was also conjectured that water condensing on the top or bottom surfaces of this spacer could have led to some of the failures. These failures were eliminated by replacing the defective spacer by that illustrated in Fig. 8, which was suggested by Dr. J. V. Harrington. The particular shape of this spacer permits it to be located some distance from the end of the center electrode (in a region of low electric field) and also reduces the possibility of a breakdown through water condensation. The use of nylon material for test units of this spacer resulted in failures, because the power absorbed was sufficient to cause them to melt. Teflon was then used and good performance was obtained.

3. Coupling Coefficient Calculation

In order to optimize the antenna gain, an equal amount of power must be coupled to each dipole. Because the amount of power in a series feed line decreases with distance from its input by the amount of power radiated up to this point, it is necessary to increase the coupling in the same proportion. The required coupling can be calculated readily, provided no reflected wave propagates in the line. This is approximately the case for long feed lines terminated in a load absorbing about 10 percent or more of the input power. In the present array, no terminating load was used in order to further maximize the gain (the last dipole is the load). There are reflected waves of appreciable amplitude in the feed line, particularly toward its end where the coupling is large, and the calculation of coupling coefficients then becomes somewhat more complicated.

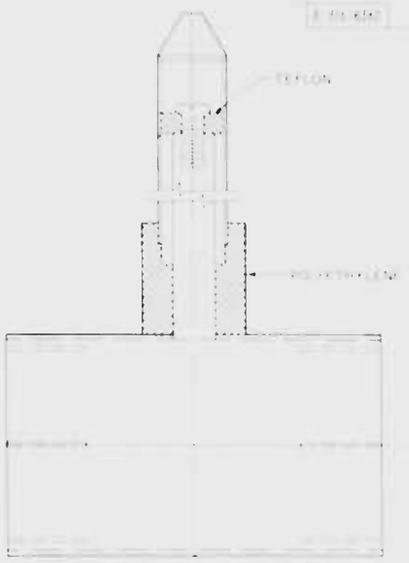

Fig. 7. Modified coupler design.

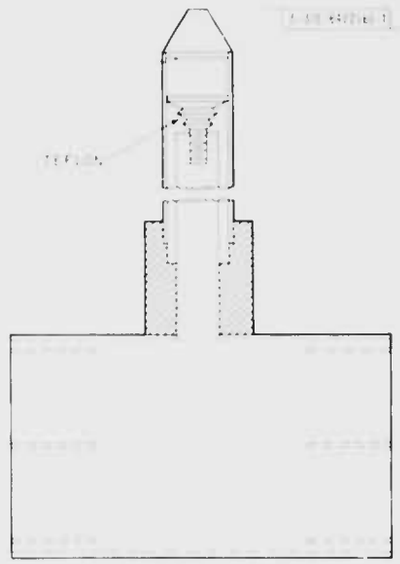

Fig. 8. Modified coupler with improved spacer.

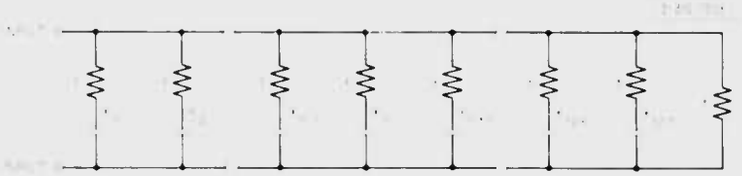

Fig. 9. Equivalent circuit diagram of feeder lines.

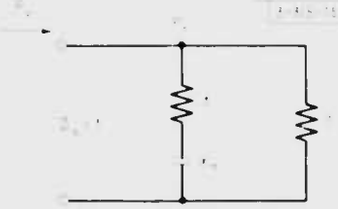

Fig. 10. Coupling coefficient measuring network.

The equivalent network of a series feed line with capacitively coupled loads is given in Fig. 9, and all impedances are normalized to the line characteristic impedance (50 ohms). The values of capacitive reactances X_n are calculated so that an equal amount of power is transferred to the dipoles, which are assumed to have a real impedance of 50 ohms. The calculation is carried out in the following manner.

Beginning with the last element (load) across which a unit voltage is assumed to exist (and therefore from which a unit power is radiated), the voltage across the preceding load is calculated. The value of the coupling capacitor for this load is calculated such that a unit power is also radiated. The reflection coefficient at this point is then calculated, and from this the voltage across the next preceding load is calculated, and so on.

The following formula relates the voltages between two successive couplers

$$V_{n-1} = V_n(1 + \alpha)\, e^{j\theta}\, [1 + \Gamma_n(1 - 2\alpha)\, e^{-j2\theta}]/(1 + \Gamma_n) \quad , \tag{2}$$

where Γ_n is the complex reflection coefficient at element n, α is the line attenuation constant per section, and $\theta = 2\pi d/\lambda$ is the electrical length between successive couplers. The reflection coefficient at coupler n (including this coupler) is given by

$$\Gamma_n = (1 - Y_n)/(1 + Y_n) \quad , \tag{3}$$

where

$$Y_n = (1 - \Gamma_{n+1}\, e^{-j2\theta})/(1 + \Gamma_{n+1}\, e^{-j2\theta}) + 1/(1 - jX_n) \tag{4}$$

and

$$X_n = [\,|V_n|^2 - 1]^{1/2} \quad , \tag{5}$$

In practice, the reactance of a coupler is measured by placing it in a line terminated by its characteristic impedance as shown in the circuit diagram of Fig. 10. The power P_n coupled to a 50-ohm load at the output of the coupler is then related to the forward power P_F by the relation

$$P_n/P_F = [X_n^2 + 2.25]^{-1} \quad . \tag{6}$$

The coupling value C_n of a coupler is defined by

$$C_n = 10 \log (P_n/P_F) \tag{7}$$

or

$$C_n = -10 \log (X_n^2 + 2.25) \quad . \tag{8}$$

Substitution into Eq. (8) of the capacitive reactance X_n found in Eq. (5) yields the required coupling values as a function of element number. The operations represented by Eqs. (7) and (8) were programmed on an IBM-7090 computer for an attenuation constant $\alpha = 0.001270$. This attenuation constant corresponds to an insertion loss of 1.4 db for the full length of the feeder line (1750 feet). The electrical spacing θ between couplers was 192°.

The calculated values of coupling as a function of coupler number are plotted in Fig. 11. The small ripple on the curve results from periodic reflections at the couplers. For comparison, the

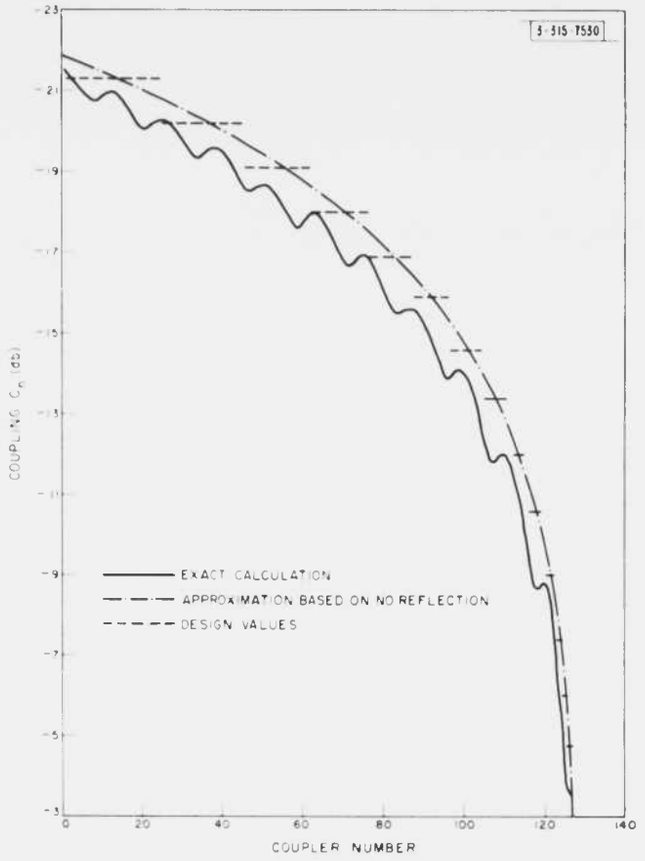

Fig. 11. Coupling coefficient as a function of coupler number.

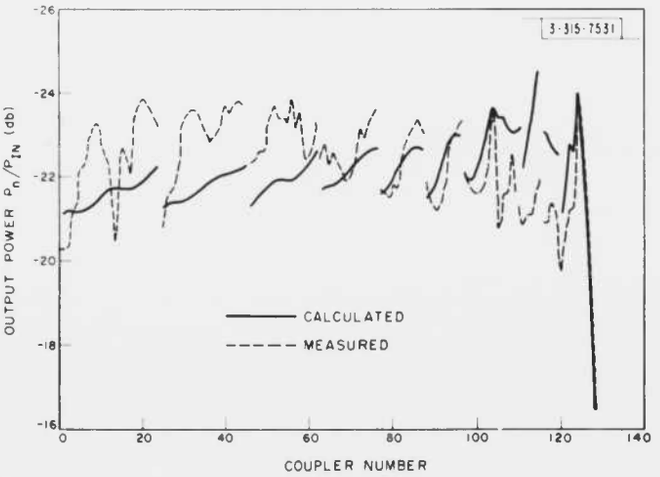

Fig. 12. Calculated and measured power at outputs of a feeder line (row 3).

coupling values obtained under the assumption that no reflection exists in the line are also plotted in Fig. 11. This coupling coefficient is given by

$$C_n = a/[(1-a)^{n-N} - 1 + a] \cong [1 - a(N-n)/2]/(N-n+1) \quad , \tag{9}$$

where C_n is the ratio of the power coupled to element n to the power in the line at element n, a is the fraction of power loss per section, and N is the total number of elements in the line. This approximation yields lower coupling values than the exact calculation.

In practice, it is necessary to reduce the number of different couplers required. This has been done by making a 1-db-step approximation of the coupling curves. The coupling design values thus obtained are indicated by dashes in Fig. 11. These design values were derived from the approximate curve because the exact calculations were not available at the time that construction of the principal array was started.

4. Power and Phase at Feeder Line Outputs

The coupling values chosen for the design differed somewhat from the required exact values, and this resulted in a slightly non-uniform distribution of power. Also, by periodically loading the feeder lines with the capacitive couplers, the wave velocity in these lines was reduced. The phase of the wave at the coupler output is related to this velocity and to the phase shift that occurs across the coupling capacitor. These two factors vary appreciably and non-uniformly along the line, principally toward its end.

The power and phase of the wave dissipated in 50-ohm loads at the feeder line terminals have been calculated for the design coupling values given in Fig. 11. The power coupled to the loads as a function of element number is plotted in Fig. 12. On this graph the coupled power is in decibels with respect to the level at the input of the feeder lines. The power coupled to the loads indicates a substantial increase toward the end of the line. This is due to a poor approximation of the ideal coupling values. Measured values of power coupled into 50-ohm loads are also shown on the graph.

The principal effect of periodically loading the feeder lines with the couplers is to increase the phase of the wave at the output of the couplers as compared with that of the unloaded line. This phase increase is plotted in Fig. 13 with respect to the phase of the voltage that appears across the last element in the line. It is observed that the increase is not linear, but becomes progressively greater toward the end of the line. This nonlinearity is corrected by appropriately changing the electrical path length in the branch lines. If left uncorrected, a reduction of gain of about 1.5 db, accompanied by a degradation of patterns, would result as shown in Sec. II-D.

Phase measurement at the coupler outputs was indirectly carried out by measuring the phase differential between successive couplers. The measured values of this quantity, together with their calculated values, are plotted in Fig. 14 for one of the feeder lines. Essentially identical results were obtained from all feeder lines. Both the power and phase measurements show variations appreciably larger than their calculated value. The following factors may account for the observed discrepancies:

(a) The couplers of the principal array were modified to improve their breakdown characteristics which may have reduced their coupling by as much as 1 db.

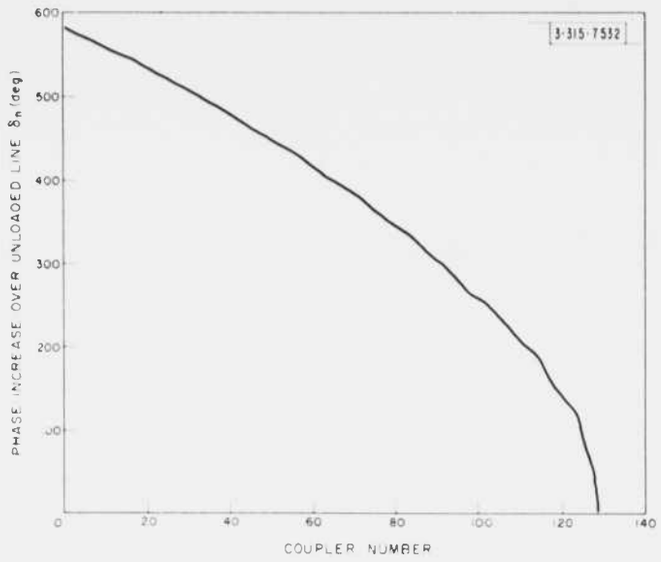

Fig. 13. Phase increase of loaded line as a function of coupler number as compared with unloaded line values.

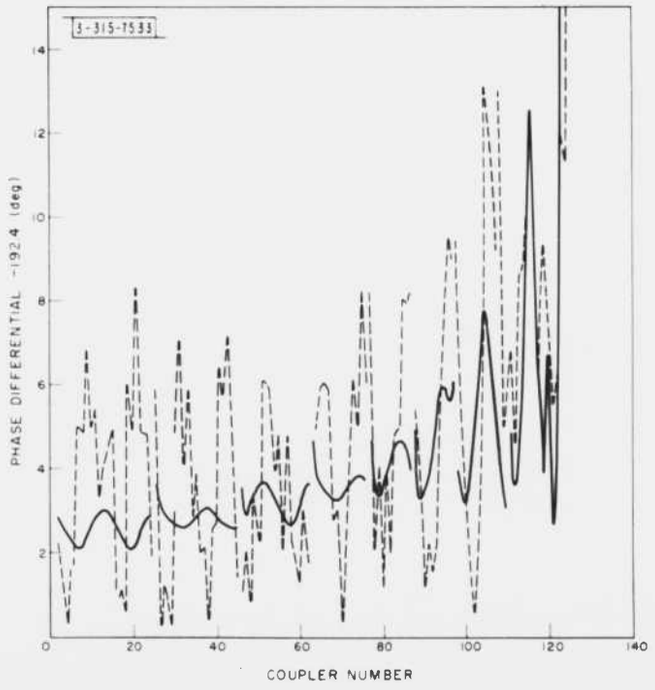

Fig. 14. Phase differential between successive couplers (row 3).

(b) The bullet connections of the principal array feed line were unsatisfactory. In various instances throughout measurements, the center conductor of some of the lines was open-circuited to DC and the RF power dropped at some bullet connections by as much as 3 db, corresponding to a series capacitive reactance of about 100 ohms. Although these extreme cases were corrected, no attempt was made to correct the lesser ones.

(c) Reflections at the supports and spacers for the center conductor were neglected in the calculation.

Furthermore, small time variations of the phase and power at the output of the couplers were observed. These variations are believed to be due to the expansion or contraction of the lines as a result of environmental changes.

5. VSWR at Feeder Line Input

The spacing between the couplers is equal to the element spacing (13.75 feet). At the design frequency this corresponds to an electrical length of 192.4°, a value sufficiently far from the resonant length to insure a low-input VSWR. The calculated value of this parameter, obtained as a by-product of the coupling and phase calculation, is about 1.20:1.0. Measured values of the main array feeder lines, with 50-ohm loads in place of the dipoles, yielded an average value of 1.22:1.00. When the antenna is operated in the normal manner, the input VSWR is also dependent on scan angle. This dependence is very slight, however, for all scan angles except at and near broadside. At broadside, the input VSWR of the feeder lines should be no greater than the VSWR in the branch lines, or about 1.5:1.0.

6. Protective Network

In a large array subjected to high input powers, a breakdown may occur in the feeder lines without any appreciable change of the power reflected to the transmitter output stages. To prevent the damages caused by such a breakdown, the feed network must include a device from which an indication of breakdown is obtained. Such a device was realized by monitoring the DC flow that results when a DC voltage is applied across the line. Since the lines are open-circuited to DC, only a leakage DC flows in normal operation, and a breakdown is indicated by a current increase which can be used to turn off the transmitter.

In order to simplify the task of finding the breakdown location, all eight feeder lines were DC decoupled to permit the application of a separate DC voltage on each of them. A DC block was installed in series with the center conductor, at the input to each line, by means of an open-circuited quarter-wave coaxial line built inside the center conductor. A high RF impedance network was provided for the application of the DC voltage to the line. This network consisted of a half-wavelength line connected in shunt with the main line and open at its far end. The DC voltage was applied at the quarter-wave point (at a voltage node).

The RF components of the protective network are shown in Fig. 15. The measured decoupling between the RF and the DC inputs is somewhat greater than 70 db.

7. The Array Element

In order to realize the specified scan capability, the array element must have a broad pattern centered on the zenith axis. The half-wave dipole best meets this requirement, and is structurally simple and relatively inexpensive to build.

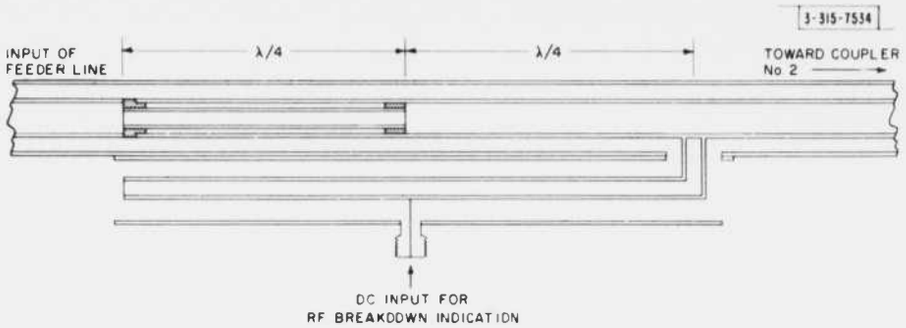

Fig. 15. Outline of RF components of protective network.

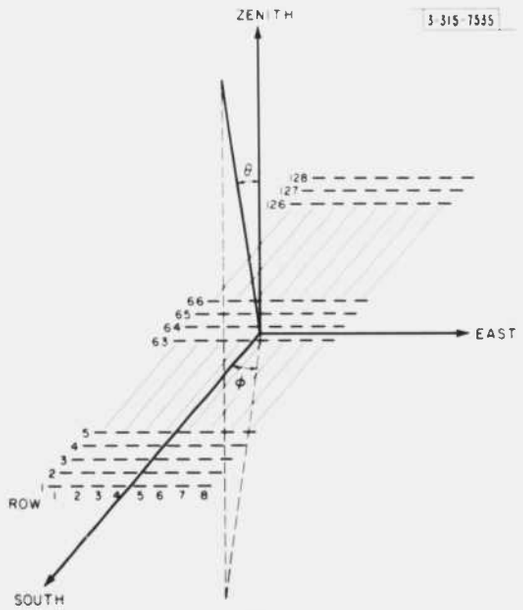

Fig. 16. Array and space coordinates.

Since the principal characteristics of the radiation pattern of a large array are controlled principally by the array factor, significant modifications of the elements have little effect on it. For instance, the length of the dipoles and their height above ground may be varied appreciably without any sizable effect on the antenna gain, beamwidth, or near side-lobe level. Such variations, however, produce appreciable changes in the dipole radiation impedance. In the present design, the length of the dipoles and their height above ground have been chosen to yield good impedance characteristics.

The impedance of a given dipole in the array is quite different from its value in the absence of the other dipoles. When placed in the array, the dipole impedance is modified by a quantity which depends on its location in the array, on its orientation, on the beam direction, and on the element spacing. However, when sufficiently remote from the edges of the array, the location factor has very little effect and all dipoles have nearly the same impedance independently of the array size.[5] In the present array, the dipoles are oriented E-W (perpendicular to the row's direction) and, except for the dipoles located on the perimeter, their impedance may be approximated by the large array value for most practical purposes. The calculated impedance of the dipoles in the array is the subject of the next section.

a. Radiation Impedance of the Dipoles

The impedance of a dipole embedded in the principal array has been calculated for practical values of dipole length and for a height above ground of 0.185λ. Impedance dependence upon scan angles was assumed to be that predicted by Edelberg and Oliner,[6] in a study based on a periodic structure approach. This dependence, for an array phased to generate a beam in a direction Θ_o, φ_o, and polarized perpendicular to the plane $\varphi = 0$ (Fig. 16), is

$$Z(\Theta_o, \varphi_o) = R(\Theta_o, \varphi_o) + jX(\Theta_o, \varphi_o) \tag{10}$$

with

$$R(\Theta_o, \varphi_o) = R(0,0)\,\sin^2(kh\cos\Theta_o)\,[\cos^2\Theta_o + \sin^2\Theta_o\cos^2\varphi_o]/[\cos\Theta_o\sin^2(kh)] \tag{11}$$

$$X(\Theta_o, \varphi_o) = X(0,0) - R(0,0)/\tan(kh) + R(0,0)\,(\cos^2\Theta_o + \sin^2\Theta_o\cos^2\varphi_o) \times \sin(2kh\cos\Theta_o)/[2\cos\Theta_o\sin^2(kh)] \quad , \tag{12}$$

where $R(0,0)$ and $X(0,0)$ are the broadside radiation resistance and reactance, respectively, h is the dipoles' height above ground, and $k = 2\pi/\lambda$. The range of usefulness of this expression has not been studied, but it is believed that it becomes inaccurate as the beam approaches directions for which a grating lobe exists.

The impedance variation for scan angles located in the meridian plane is of principal interest because, for most applications, the beam is located in this plane. This is obtained by making $\varphi_o = 0$ in Eq. (10) and is

$$Z(\Theta_o, 0) = R(0,0)\,\sin^2(kh\cos\Theta_o)/\cos\Theta_o\sin^2(kh) + j[X(0,0) - R(0,0)/\tan(kh) + R(0,0)\,\sin(2kh\cos\Theta_o)/(2\cos\Theta_o\sin^2(kh)] \quad . \tag{13}$$

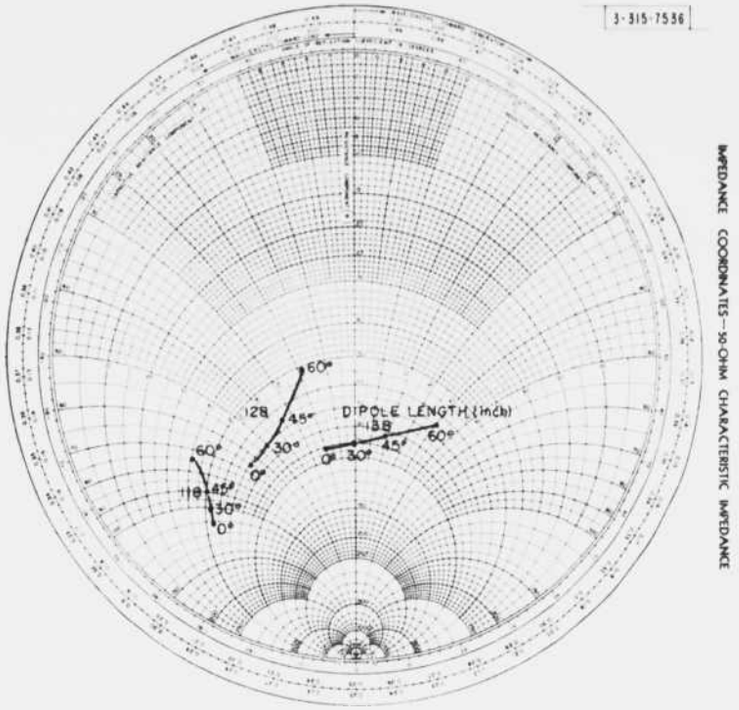

Fig. 17. Feed point impedance af a dipole element inside the infinite array (dipole diameter = 1.75 inches).

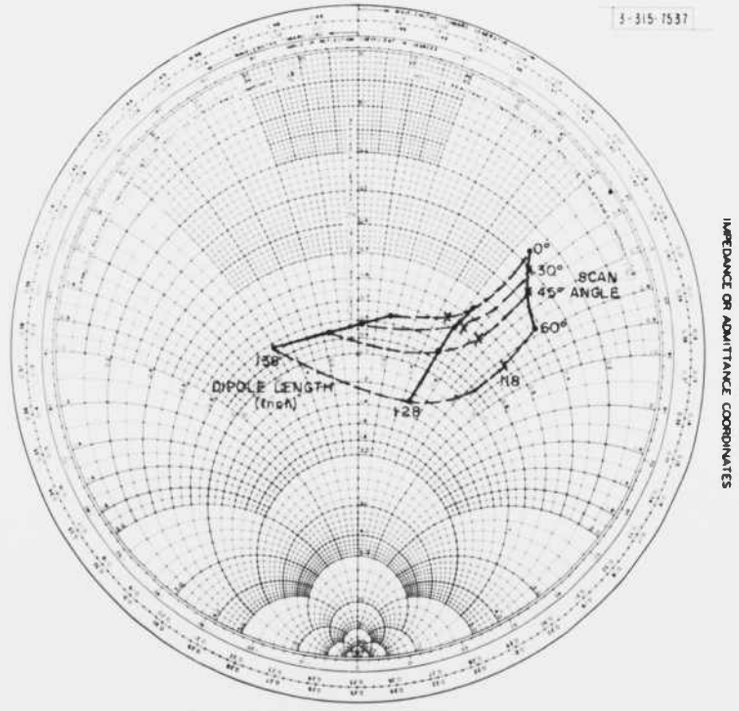

Fig. 18. Feed point odmittonce normalized to 13.3 milliohms of o dipole element inside the infinite orray (dipole diameter = 1.75 inches).

The radiation resistance and reactance at broadside were taken to be that of the center dipole of a 3 × 3 uniform array. To the authors' knowledge, values of mutual impedances between near-resonant-finite cross-section dipoles have been published for parallel side-by-side dipoles only.[7] For the staggered and collinear dipoles of the 3 × 3 array, mutual impedances were approximated from their value for the infinitely thin resonant dipoles. The resulting dipole base impedance as a function of scan angle is plotted on a Smith chart for three values of dipole length (Fig. 17). This plot is believed to be accurate within about 10 percent.

b. Matching Network

The previous feed-point (or base) impedance calculation applies to a dipole embedded in a large array in which all dipoles are excited by currents of equal amplitude, or in which the amplitude variation from element to element is so small as to be considered constant. In the present array, this is not the case. The amplitude of the current in the dipoles depends on the amount of power coupled from the feeder lines to the branch lines which, in turn, depends on the impedance at the couplers' output, looking toward the dipoles. As the length of the branch lines varies from element to element to produce the required phase taper, this impedance varies whenever reflected waves exist in the branch lines. Under this condition, the dipoles are non-uniformly excited and their impedance becomes a function of position in the array. The calculation of dipole impedances in the presence of mismatches in the branch lines is very complex and has not been attempted. However, measurements have shown that the impedance variation with scan angle is appreciably larger than that predicted on the basis of equal dipole currents (Fig. 17). For instance, when the dipoles' length is set at 138 inches and a quarter-wavelength 75-ohm transformer is interposed between each dipole and the 50-ohm phasing cable, a VSWR of about 1.25 for a scan angle of 30° and only 1.8 for 52.5° may be expected when equal currents flow in all dipoles. However, in the actual array, the relationship between the dipole currents is so altered by the mismatches that a much larger change of VSWR occurs. The measurements described in a later section indicate that this change is so drastic in some cases that elements are found which absorb power instead of radiating it.

To prevent high element mismatches at any of the scan angles of operation, each element was provided with a dual-parameter matching network. This network consists of a quarter-wavelength 75-ohm transformer and a shorted stub shunted across the dipole feed point (see Fig. 2). The length of this stub is variable and so is the dipole length. The operation of this network may be understood by referring to Fig. 18, where the data of Fig. 17 are replotted in terms of admittance normalized to 13.3 milliohms (Z_o = 75 ohms). In order for the impedance at the transformer input to be 50 ohms, the impedance appearing at the other end must be 112.5 ohms, or the admittance must be 0.66 when normalized to 13.3 milliohms. At any of the scan angles of interest, the dipole length may be adjusted so that its normalized conductance will be 0.66. By shunting a stub of proper inductive susceptance across the dipole feed point, a perfect match is realized for this scan angle. The shunt stub consists of a parallel line made of 1/2 × 1/2 inch angle aluminum spaced about 3.5 inches. The measured characteristic impedance of the line is 285 ohms. The stub and dipole lengths required to provide a match for practical beam directions located in the meridian plane are plotted in Fig. 19.

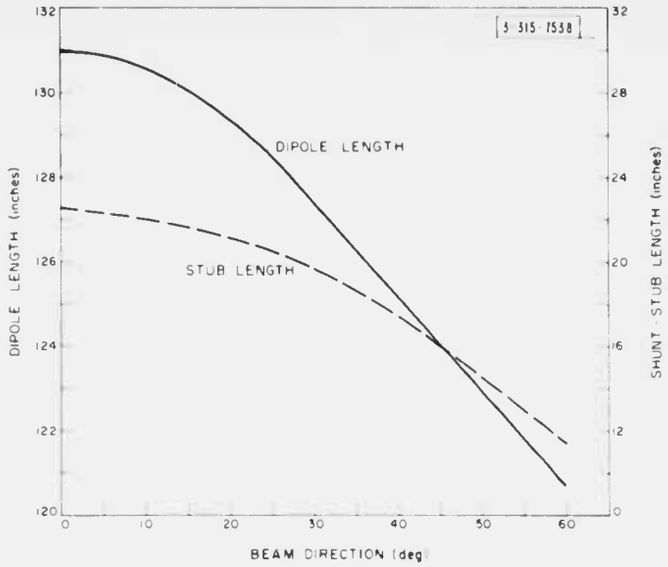

Fig. 19. Stub and dipole lengths required to match the element impedance to 50 ohms as a function of beam direction.

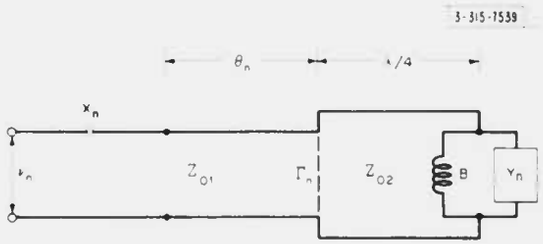

Fig. 20. Equivolent circuit of bronch lines with dipoles.

c. Effects of Mismatches in the Branch Lines

The phase of the excitation current of each element is adjusted in the branch lines. The electrical length of these lines is therefore a function of the required beam direction and of the element location of the array. When scanning in the N-S plane, the dependence on location is a function of the position in a row only. This function varies in a sawtooth manner with a "phasing period" equal to the number of elements over which the phase increases by 360°. When a reflected wave exists in the phasing cables, the excitation of the dipoles is not uniform because of the varying impedances reflected at the couplers. The effect of mismatches in the branch line on pattern and gain can be estimated in the following way.

The circuit representation of the branch lines is given in Fig. 20. The current in dipole n may be shown to be

$$i_n = \frac{v_n \exp[-j\Theta_n]\left[1 + jB\frac{Z_{02}^2}{Z_{01}}\right]\left\{1 + \Gamma_n \exp\left[-j2\tan^{-1}\frac{BZ_{02}^2}{Z_{01}}\right]\right\}}{Z_{02}\{1 - jX_n\}\{1 + \Gamma_n \exp[-j2(\Theta_n - \tan^{-1}X_n)]\}} \quad , \tag{14}$$

where Θ_n is the electrical length of the phasing cable to element n, v_n is the voltage across the feeder line at coupler n, X_n is the capacitive reactance of that coupler normalized to 50 ohms, Z_{01} is the phasing cable characteristic impedance (50 ohms), Z_{02} is the quarter-wave transformer characteristic impedance (75 ohms), B is the stub inductive susceptance, and Γ_n is the complex reflection coefficient at the driving point and is equal to

$$\frac{\frac{Z_{02}^2}{Z_{01}}(Y_n - jB) - 1}{\frac{Z_{02}^2}{Z_{01}}(Y_n - jB) + 1} \quad , \tag{15}$$

where Y_n is the radiation admittance of dipole n.

For most of the line couplers $X_n \gg 1$* and for all scan angles of interest, $B \cong Z_{01}/Z_{02}^2$. Furthermore, the power reflected back from the branch lines into their feeder line may be neglected for most of the line length since the coupling value is small. Under these conditions, the current in dipole n is

$$i_n \cong \frac{i_o[1 - j\Gamma_n]\exp[-j\Theta_n]}{(1 - \Gamma_n \exp[-j2\Theta_n])} \quad , \tag{16}$$

where i_o is the uniform current flowing in all dipoles when $\Gamma_n = 0$. The complete solution for i_n involves the knowledge of the Γ_n, which is a function of the feed-point impedance of the n^{th} dipole. This impedance is a function of the mutual impedances with all other dipoles and could be approximated by taking account of the mutual effects from the nearest ones only. Solution of this problem was not attempted, since the mismatches were generally small and not too detrimental, as shown in the following analysis.

Measurements of VSWR in the branch lines indicated that the amplitude of the reflection coefficient varies about a mean value with a period that corresponds to the "phasing" period. No

*X_n is roughly proportional to $\sqrt{128 - n}$.

measurement of its phase has been made, but this latter may also be assumed to vary periodically about some mean value, and with the same period as the amplitude variation. The effect of mismatches in the phasing cables may then be approximated by replacing the complex reflection coefficient in Eq. (16) by its average value. (The effects of variations of this coefficient on the radiation pattern and gain are thus assumed to be small and are neglected.) The dipole currents then become

$$i_n \simeq \frac{i_o[1 - j\bar{\Gamma}] \exp[-j\Theta_n]}{(1 - \bar{\Gamma} \exp[-j2\Theta_n])} \quad . \tag{17}$$

For small reflections this may be expanded to yield

$$i_n \simeq i_o[1 - j\bar{\Gamma}] \{\exp[-j\Theta_n] + \bar{\Gamma} \exp[-j3\Theta_n] + \bar{\Gamma}^2 \exp[-j5\Theta_n], \ldots\} \quad . \tag{18}$$

The dipole currents are a series of progressively delayed waves of complex amplitude proportional to $1, \bar{\Gamma}, \bar{\Gamma}^2, \bar{\Gamma}^3, \ldots$. The pattern resulting from such an excitation is therefore the sum of a series of patterns of identical characteristics, but of different amplitudes and beam directions. The array factor of these patterns is in the proportion $1, |\bar{\Gamma}|^2, |\bar{\Gamma}|^4 \ldots$, while their beam directions are related to the phase differential between successive elements $(\Theta_n - \Theta_{n-1})$, $3(\Theta_n - \Theta_{n-1})$, $5(\Theta_n - \Theta_{n-1})$, etc. This series of progressively delayed currents may be interpreted as the series of waves which results from multiple reflections between a mismatch dipole and the high impedance coupler. The single delayed wave generates the desired beam and the multiple delayed ones generate spurious beams. For the small mismatches occurring in the array, only the first of these multiple delayed waves is of appreciable amplitude. It will produce a spurious beam in a direction related to the principal beam direction as given in Fig. 21. The peak of this spurious beam is related to that of the principal beam by the square of the average value of the reflection coefficient and by the relative directivity of the element pattern in the directions of the respective peaks. In general, the principal beam is separated from the spurious beam by many beamwidths, and will therefore produce little distortion of the principal beam. The pattern measurements described in Sec. II-D indicate clearly the first spurious beam, and its location and amplitude agree well with prediction.

Although mismatches in the branch lines do not affect the principal beam shape, they reduce the power radiated in its direction. The gain reduction may be obtained by calculating the amount of power in the fundamental component of the dipole current. This is found to be

$$\frac{P_o}{N} (1 - |\bar{\Gamma}|^2) \quad , \tag{19}$$

where P_o is the input power to the array and N is the total number of elements. The power transmitted in the direction of the principal beam is decreased by an amount proportional to the square of the average value of the reflection coefficient.

The power coupled to the dipoles, when mismatch exists in the branch lines, varies from element to element. It is convenient, in practice, to measure the respective power of the forward and reverse waves in the branch lines by means of a directional coupler, and to deduce VSWR from their ratio. These powers are proportional to the square of the amplitude of the respective waves. When the reflection coefficient is replaced by its average value, the forward wave power is, for small values of this coefficient,

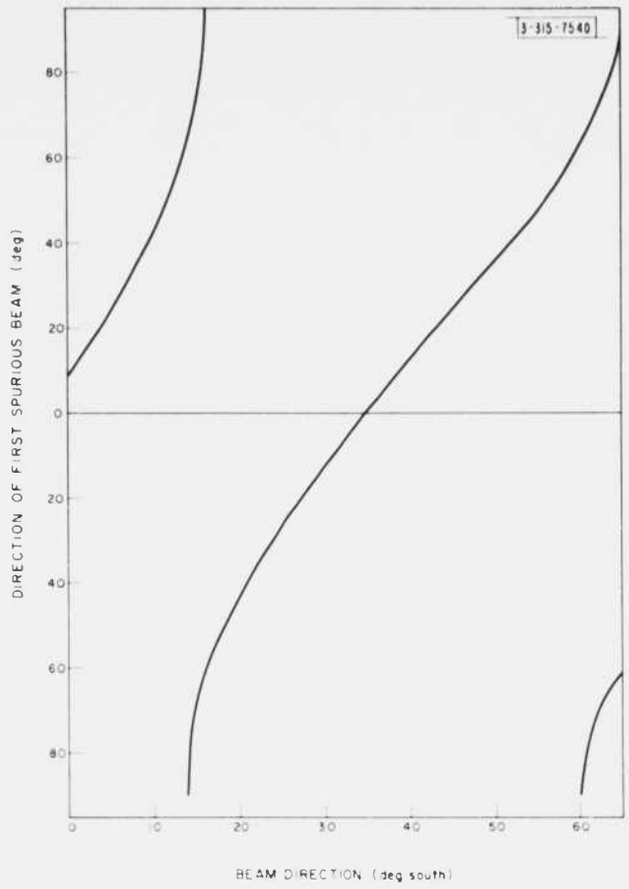

Fig. 21. Direction of first spurious beam as a function of beam direction.

$$P_F \simeq \frac{P_o}{N} [1 + |\bar{\Gamma}|^2 + 2|\bar{\Gamma}| \cos \Theta_n] \quad . \tag{20}$$

The electrical length Θ_n is proportional to the element number; therefore, the forward wave power, as a function of element number, is periodic and its period corresponds to the phasing period. Measured values of this power do not vary exactly as predicted by Eq. (20) because the reflection coefficient is not constant from element to element.

d. Measured VSWR and Relative Power of Forward Wave in Branch Lines

The power coupled to the dipoles is uniform (to the accuracy of the design values) only when no mismatch exists in the branch lines. However, a mismatch does exist for some of or all the following reasons:

(1) The same matching network is used for all the dipoles, even though the elements on the edges of the array have impedances appreciably different from that of the other elements.

(2) The height of the dipole above the ground plane varies by ±6 inches.

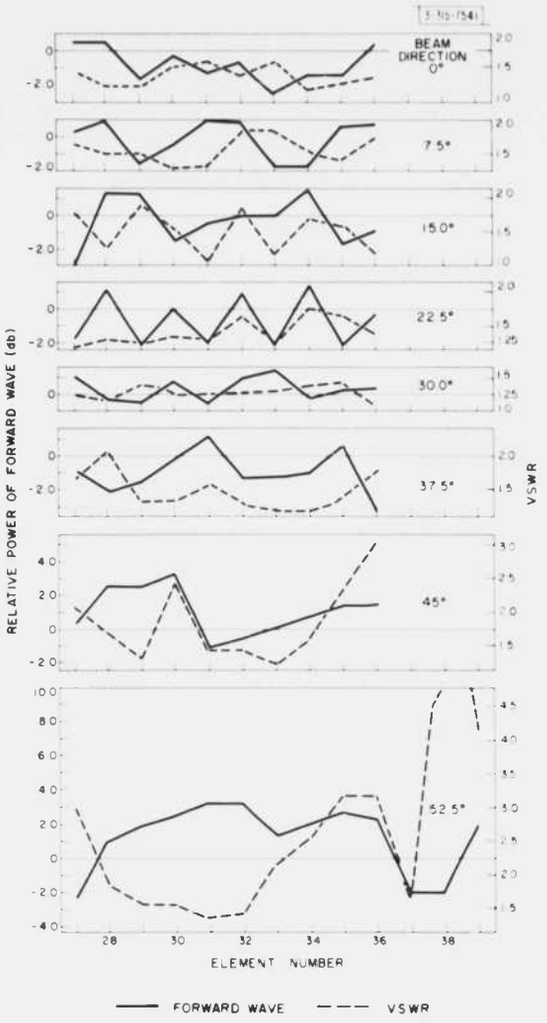

Fig. 22. Relative power af farward wave and VSWR in a few successive branch lines of raw 5. Dipole length 128 inches, stub length 34 inches.

Fig. 23. Relative power af farward wave and VSWR in a few successive branch lines af raw 5. Dipole length 123 inches, stub length 17 inches.

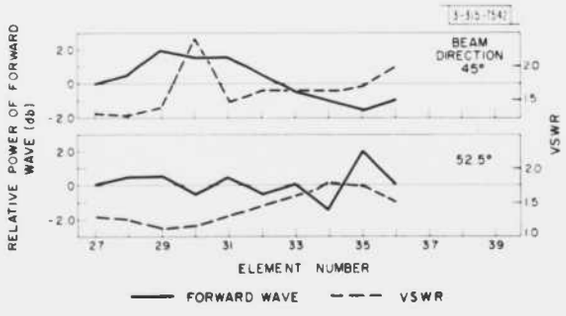

(3) The setting of the matching network is based on calculated values of dipole impedance, which are approximate and in which the effects of dipole supports and of the feed-line structure have been neglected.

The forward wave power and the VSWR in the branch lines were measured for a representative section of the array. This section consisted of elements 27 to 36 of rows 1, 3, 5, and 7. The measurements were taken with the array phased to generate beams at different scan angles of 0°, 7.5°, 15°, 22.5°, 30°, 37.5°, 45°, 52.5° – all in the southern part of the meridian plane.

These measurements were made to determine the angle range over which the beam could be scanned without detrimental effects when the matching network parameters were fixed. The limit of scan is principally determined by the condition that the power level in the phasing cables should not exceed their peak carrying capacity. Under uniform excitation, each of these cables carries a power of about 400 watts. When there is a standing wave in these cables, the power level at the peak of the wave is

$$P_{peak} = 400 \cdot \left(\frac{1 + |\Gamma|}{1 - |\Gamma|}\right)^2 = 400[\text{VSWR}]^2 \text{ watts} \qquad (21)$$

This peak power level exists only if the correct combinations of phasing cable length and reflection coefficient phase occur at a given element. The power-carrying capacity of the phasing cables (RG-8/U) is conservatively rated at 1500 watts at 40 Mcps. This value has been exceeded slightly by allowing peak values of VSWR as high as 2.0:1.0 to exist.

The VSWR measurements in the branch lines were obtained as follows. The matching network parameters were first set to the calculated values (Fig. 19) for a scan angle of about 30° and the VSWR was measured over the representative array referred to above ($\times$ 8 array).* These measurements were performed when the excitation current of the elements of only one part of the array was phased properly. The size of the array chosen for this purpose was such that no change in measurement was observed by increasing it. Only a few extra elements at both ends of the 10 × 8 array needed to be added. Actually, elements 25 to 38 were excited properly (14 × 8 array) and measurements made on elements 27 to 36 of the odd rows. Excitation of the remaining elements produced a beam close to broadside for all measurements. Fairly identical results were obtained on all rows. Typical measurements obtained on row 5 are plotted in Fig. 22 for eight values of the scan angles. It is seen that for scan angles down to 45°, the chosen dipole and stub lengths yield acceptable results. At 45°, the VSWR was larger than 2.0:1.0 on some elements. At 52.5°, it was so bad that some elements were actually found to absorb power instead of radiating it. The matching network parameters were then changed to the set of values required to provide a match for a scan angle of 48° and the VSWR of the same elements as above again measured for scan angles of 45° and 52.5°. The results for row 5 are given in Fig. 23. Satisfactory results are obtained at the low scan angles with this setting.

The array has been operated at full power over most declination angles in the range 7.5° south to 52.5° south in steps of 0.20°. The matching network parameters of the elements were those of Fig. 22 for scan angles from 7.5° to 42° and those of Fig. 23 for scan angles from 42° to 52.5°. No cable failures due to a high mismatch were experienced throughout these tests.

---

*Because of some misunderstanding, the length of the shunt stub was set to a value larger than that referred to.

8. Ground Plane

The area in which the array is placed can, in general, be described as flat. In the N-S direction, it is sloped downward approximately two minutes to the south. In the E-W direction, there is a downward slope of about 0.5° toward the east. Neither one of these was enough to require general re-leveling of the entire field. However, there were some discrete mounds and valleys which had been plowed into this field, formerly used for rice growing, and these had to be removed. The original specifications required that the ground be level within ±3 inches. After an attempt to do this, when the condition of the ground varied from a sea of mud to concrete-like hardness, the specifications were relaxed by reducing the tolerance to ±6 inches.

To improve the ground reflectivity, a conducting screen was laid over it which consisted of a galvanized mesh "chicken wire," hexagonal in shape with each side approximately two inches long. The screen was laid over the entire area and extended beyond the end of the edge elements for 10 feet.

C. Calculated Directivity Patterns and Estimated Gains

The radiation patterns of the array are studied by considering first the patterns of the uniformly excited array and second, the modifications of these patterns caused by known deviations from a uniform excitation. These deviations are:

(1) A superimposed amplitude ripple resulting from approximate design values of the couplers and non-uniformities in the series feed lines.

(2) A superimposed phase ripple of ±11.25° due to the quantization of the branch lines phase shifters.

(3) Mismatches in the branch lines which give rise to a series of multiple delayed waves.

The random variations due to manufacturing tolerances are very small in terms of a wavelength and their effects are not considered.

1. Radiation Patterns of the Uniformly Excited Array

The far field of the uniformly excited array, expressed in terms of its directivity $D(\Theta, \varphi)$ – the ratio of the array field intensity in the direction Θ, φ to that of an isotropic radiator transmitting an equal amount of power – is nearly identical to

$$D(\Theta, \varphi) = \frac{480\, N_1 N_2 \sin^2 kh}{R(\Theta_o, \varphi_o)} \left[\frac{\sin(kh \cos\Theta) \cos(\frac{\pi}{2} \sin\Theta \sin\varphi)}{(1 - \sin^2\Theta \sin^2\varphi)^{1/2} \sin kh} \right]^2$$

$$\cdot \left[\frac{\sin(N_1 u_1/2) \sin(N_2 u_2/2)}{N_1 \sin(u_1/2)\, N_2 \sin(u_2/2)} \right]^2 , \qquad (22)$$

which is the directivity of a similar array of thin half-wave dipole elements. (The effect, on the element pattern, of the presence of the other dipoles is neglected.)

In Eq. (22) $R(\Theta_o, \varphi_o)$ is the radiation resistance of each array element in the presence of all other elements properly phased to scan the beam in a direction Θ_o, φ_o; N_1 is the number of rows and N_2 is the number of elements per row. The parameters u_1 and u_2 are, respectively,

$$u_1 = \frac{2\pi}{\lambda} d \sin\Theta \sin\varphi + \beta \tag{23}$$

$$u_2 = \frac{2\pi}{\lambda} d \sin\Theta \cos\varphi + \alpha \quad , \tag{24}$$

where d is the uniform spacing, and α and β are the uniform phase increment measured along and across the rows, respectively.

The radiation pattern is more conveniently discussed by separating the element and the array factors from the directivity function. The normalized element factor

$$\frac{\sin^2(kh \cos\Theta) \cos^2[\frac{\pi}{2} \sin\Theta \sin\varphi]}{\sin^2(kh)\,(1 - \sin^2\Theta \sin^2\varphi)} \tag{25}$$

is plotted in Fig. 24 for $\varphi = 0°$, 30°, 60°, and 90°. The normalized array factor

$$\frac{\sin^2(N_1 u_1/2)}{N^2 \sin^2(u_1/2)} \quad \frac{\sin^2(N_2 u_2/2)}{\sin^2(u_2/2)} \tag{26}$$

is a function with a peak value equal to 1 ($N = N_1 N_2$ the total number of elements) whenever

$$u_1 = \frac{2\pi}{\lambda} d \sin\Theta \sin\varphi + \beta = 0, \pm 2\pi, \pm 4\pi, \ldots \tag{27}$$

and

$$u_2 = \frac{2\pi}{\lambda} d \sin\Theta \cos\varphi + \alpha = 0, \pm 2\pi, \pm 4\pi, \ldots \tag{28}$$

simultaneously. In general, only a few solutions of u_1 and u_2 yield real values of Θ, φ. For the present array there are only two solutions, one corresponding to the beam direction and the other to the grating lobe direction as discussed in Sec. II-B-1.

To produce a beam in a direction Θ_0, φ_0, the progressive linear phase shift along and perpendicular to the rows must be

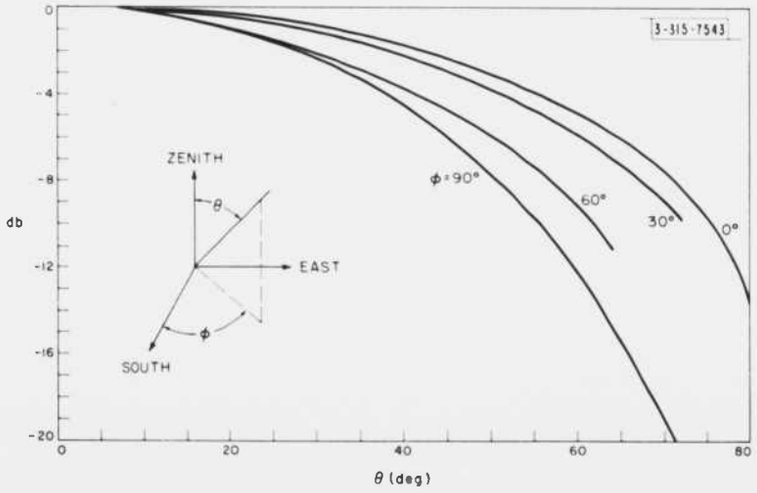

Fig. 24. Radiation patterns of principal array element.

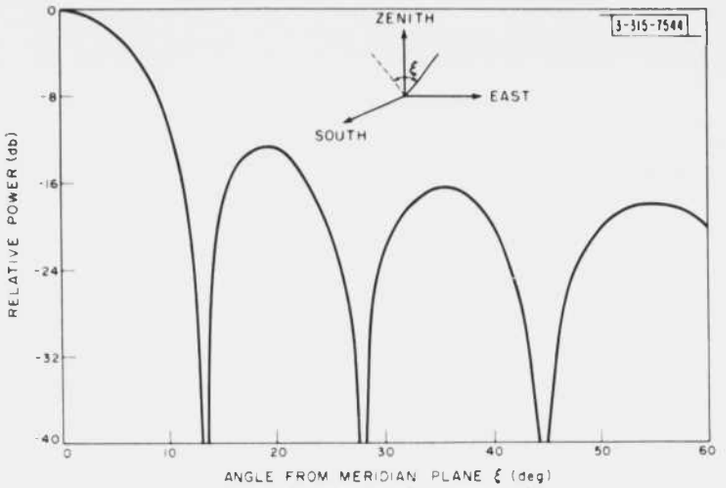

Fig. 25. Array factor an canes coaxial to N-S axis far beam directions located in the meridian plane.

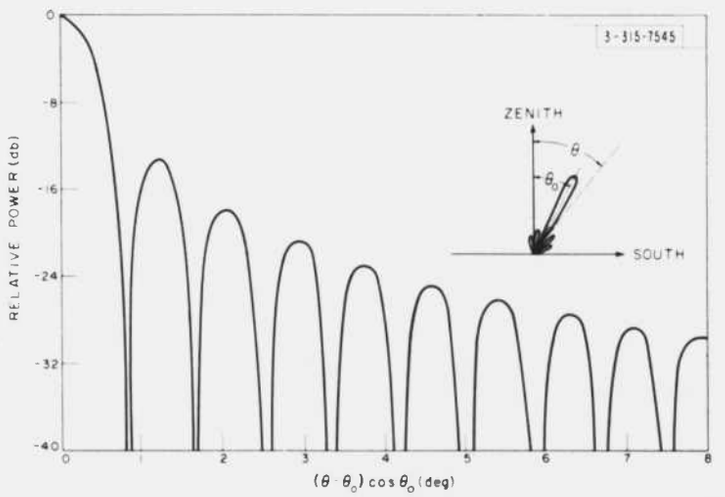

Fig. 26. Array factor in meridian plane for beam directions located in this plane.

$$\alpha = 2\pi \left[\pm m_1 - d/\lambda \sin\theta_o \cos\varphi_o \right] \tag{29}$$

$$\beta = 2\pi \left[\pm m_2 - d/\lambda \sin\theta_o \sin\varphi_o \right] \quad , \tag{30}$$

respectively, where m_1 and m_2 are any integers. With these values of α and β, the array factor becomes

$$\frac{\sin^2 \frac{N_1 \pi d}{\lambda} (\sin\theta \sin\varphi - \sin\theta_o \sin\varphi_o) \sin^2 \frac{N_2 \pi d}{\lambda} (\sin\theta \cos\varphi - \sin\theta_o \cos\varphi_o)}{N^2 \sin^2 \frac{\pi d}{\lambda} (\sin\theta \sin\varphi - \sin\theta_o \sin\varphi_o) \sin^2 \frac{\pi d}{\lambda} (\sin\theta \cos\varphi - \sin\theta_o \cos\varphi_o)} \quad . \tag{31}$$

The behavior of the array factor when the beam axis is located in the meridian plane ($\varphi_o = 0$) is of principal interest. The array factor now becomes

$$\frac{1}{N^2} \left[\frac{\sin^2 \left(\frac{N_1 \pi d}{\lambda} \sin\theta \sin\varphi \right)}{\sin^2 \left(\frac{\pi d}{\lambda} \sin\theta \sin\varphi \right)} \right] \left[\frac{\sin^2 \left(\frac{N_2 \pi d}{\lambda} \right) (\sin\theta \cos\varphi - \sin\theta_o)}{\sin^2 \left(\frac{\pi d}{\lambda} \right) (\sin\theta \cos\varphi - \sin\theta_o)} \right] \quad , \tag{32}$$

and is the product of two functions. It is best described by considering the behavior of one function in directions for which the other is maximum. The second of these functions is maximum for directions given by

$$\sin\theta \cos\varphi = \sin\theta_o \quad . \tag{33}$$

The locus of these directions is a cone of angle $\pi - 2\theta_o$ centered on the row axis. The normalized power density on this locus is

$$\frac{\sin^2 \left(\frac{N_1 \pi d}{\lambda} \sin\xi \right)}{N_1^2 \sin^2 \left(\frac{\pi d}{\lambda} \sin\xi \right)} \quad , \tag{34}$$

where ξ is the direction angle measured from the meridian plane. This function is plotted in Fig. 25 for $N_1 = 8$ and $d/\lambda = 0.5343$. For a beam directed toward zenith, this function multiplied by the element factor is the array pattern in the E-W plane.

The first function of the array factor in Eq. (32) is maximum for

$$\sin\theta \sin\varphi = 0 \quad \text{occurring when } \varphi = 0 \tag{35}$$

(in the meridian plane). The normalized power density in this plane is

$$\left[\frac{\sin N_2 \frac{\pi d}{\lambda} (\sin\theta - \sin\theta_o)}{N_2 \sin \frac{\pi d}{\lambda} (\sin\theta - \sin\theta_o)} \right]^2 \quad . \tag{36}$$

For small angles from the beam axis and for large values of N_2, Eq. (36) may be approximated to

$$\left[\frac{\sin \frac{N_2 \pi d(\theta - \theta_o) \cos\theta_o}{\lambda}}{\frac{N_2 \pi d(\theta - \theta_o) \cos\theta_o}{\lambda}} \right]^2 \tag{37}$$

which is plotted in Fig. 26 as a function of $(\theta - \theta_o) \cos\theta_o$ for $N_2 = 128$ and $d/\lambda = 0.5343$. Since

this function varies rapidly with angle whereas the element factor varies quite slowly, the radiation pattern in the vicinity of the beam is very closely that of Fig. 26. At larger angles away from the beam, the element directivity must be taken into account and Eq. (36) must be used.

The beamwidth in the meridian plane is readily found to be

$$\text{Beamwidth} \cong \frac{0.74^\circ}{\cos \Theta_o} \quad . \tag{38}$$

The accuracy of this expression decreases with scan angle, but is still better than 0.3 percent at 60°.

For a more complete discussion of the array factor of uniformly excited planar arrays, the reader is referred to Allen, et al.[8]

a. Calculation of Phasing Cable Lengths

The required increment between the current phase of adjacent elements, so that the beam is formed in a direction Θ_o in the meridian plane, is given by Eqs. (29) and (30), with $\varphi_o = 0$ and $m_1 = m_2 = 0$. The result is

$$\alpha = -\frac{2\pi d}{\lambda} \sin \Theta_o \quad \text{and} \quad \beta = 0 \quad . \tag{39}$$

For practical reasons, the corresponding cable incremental lengths have been calculated with respect to the last element of a row. The phase difference between the exciting current of element n with respect to the last element is then required to be

$$-(128 - n)\alpha = (128 - n)\frac{2\pi d}{\lambda} \sin \Theta_o \quad . \tag{40}$$

This phase difference is made up of the phase difference between the voltages at the output of the last coupler and that at coupler n, plus the phase shift that results from the length increment between the corresponding branch lines. The first of these has been calculated in Sec. II-B-3 and is given by

$$-(128 - n)\frac{2\pi d}{\lambda} - \delta_n \quad , \tag{41}$$

where δ_n is given by the curve of Fig. 13, and the second is Φ_n. Therefore,

$$-(128 - n)\frac{2\pi d}{\lambda} - \delta_n + \Phi_n = (128 - n)\frac{2\pi d}{\lambda} \sin \Theta_o$$

or

$$\Phi_n = (128 - n)\frac{2\pi d}{\lambda}[1 + \sin \Theta_o] + \delta_n \quad . \tag{42}$$

The approximated incremental lengths in terms of multiples of a one-sixteenth wavelength, $m(\lambda/16)$, is

$$m(\lambda/16) = \frac{(128 - n)\frac{2\pi d}{\lambda}(1 + \sin \Theta_o) + \delta_n}{\pi/8} \quad , \tag{43}$$

rounded off to the nearest integer and reduced by the multiples of a wavelength which it contains.

The calculation of the cable lengths required in each branch line to direct the beam in any direction from 60° north to 60° south in steps of 0.2° has been performed with the help of the 7090 computer.

b. Peak Directivity

The peak directivity of the uniformly excited array is obtained by making $\Theta = \Theta_o$ and $\varphi = \varphi_o$ in Eq. (22) and replacing the radiation resistance by its expression as obtained in Eq. (11). The result is

$$D(\Theta_o, \varphi_o) = \frac{480\ N \cos^2 [\frac{\pi}{2} \sin \Theta_o \sin \varphi_o] \cos \Theta_o \sin^2 kh}{R(0,0)\ [\cos^2 \Theta_o + \sin^2 \Theta_o \cos^2 \varphi_o]\ [1 - \sin^2 \Theta_o \sin^2 \varphi_o]} \quad , \tag{44}$$

where $R(0, 0)$ is the broadside radiation resistance of each element in a similar array of infinitely thin half-wavelength dipoles. In the meridian plane of scan, the peak directivity is

$$D(\Theta_o, 0) = \frac{480\ N \sin^2 kh}{R(0,0)} \cos \Theta_o \quad . \tag{45}$$

The accuracy of the angular dependence of this expression is directly linked to that of the radiation resistance expression used to derive it. The authors believe that it becomes inaccurate for scan angles approaching directions for which a grating lobe is formed.

The broadside radiation resistance of each element of a similar array of infinitely thin half-wave dipoles is well approximated by the value of the center element of a 7×9 array.[9] This value is about 110 ohms, and when it is inserted in Eq. (45), together with $N = 1024$ and $h = 0.185\lambda$, the directivity becomes

$$D(\Theta_o, 0) = 3740 \cos \Theta_o \quad , \tag{46}$$

or 35.7 db for the broadside beam.

Wheeler[10] has shown that the peak directivity of a uniformly excited array, with the elements spaced so that only one principal beam exists in the real domain, is also given by the well-known formula for the peak directivity of a uniformly illuminated aperture

$$D(0, 0) = \frac{4\pi A}{\lambda^2} \quad , \tag{47}$$

where A is the area aperture. When the array parameters are substituted in Eq. (47), the peak directivity of the broadside beam is 35.6 db, which corroborates well the theoretical prediction. For other beam directions located in the meridian plane, the peak directivity is, from Eqs. (45) and (47), equal to that of the aperture projected in these directions.

2. Effects of Deviations from Uniform Excitation on Pattern and Directivity

The principal effects of the deviations listed at the beginning of this section on the patterns and gain are:

> Non-Uniform Amplitude Distribution:– The power coupled to each branch line varies as shown previously in Fig. 12. A more-or-less sinusoidal ripple modulates the curve of coupled power as a function of element number. The peak-to-peak amplitude of this ripple is about 1.2 db and its period is about 11 elements. Furthermore, the last 20 percent of the elements of each row have a progressively increasing amount of power delivered to them, and the power in the last element is about 6 db larger than the average value of the power coupled to each element.
>
> The effect of the ripple has been estimated by assuming it to be sinusoidal. The principal effect is to raise the level of two side lobes, one on each side of the beam and located near the eleventh side lobe, to a value about 25 db

below the peak of the beam. The level of these side lobes is 6 db higher than their level in the absence of the sinusoidal perturbation. The excess power in these side lobes decreases the power in the main beam by about 0.04 db. The main effect of the excess power delivered to the end of the array is to reduce the gain by an estimated 0.1 db and to slightly increase the beamwidth (2 percent).

Phase Ripple:– The effect of quantizing the phase shifters is to perturb the required progressive phase distribution by superimposing a sawtooth ripple. The amplitude of this ripple is 22.5° peak to peak. Its period is a function of the difference between the required phase increment and the quantized value and varies with the beam direction. The principal effect of the phase ripple is, like the amplitude ripple, to raise the level of two side lobes one on each side of the beam. The location of these side lobes and their amplitude is a function of scan angles. For most scan angles, the level of these side lobes is 20 db or more below the peak of the beam and the maximum gain reduction that may result is about 0.2 db.

Mismatches in the Branch Lines:– Figures 22 and 23 showed that the average VSWR in the branched line is about 1.5:1.0. This corresponds to a reflection coefficient of 0.2. It was further shown in Sec. 11-7-c that the effect of mismatches in the branch lines is to split the exciting current into a series of multiple delayed currents of progressively smaller amplitude which correspond to the multiple reflections between the coupler and the radiating element. For small mismatches, only the first multiple delayed wave is significant. The delay of this wave is three times that of the fundamental wave and the beam it generates is at least 14 db below the main beam. The location of this beam is related to that of the principal beam, as was shown in Fig. 21. The power radiated in secondary beams reduces the power in the main beam by about 0.2 db.

3. Calculated Gain

The antenna gain is equal to the peak directivity of the ideal array reduced by losses due to deviations from the ideal excitation, or radiation losses, and by those inherent to the feed system or conduction losses. These losses are:

Radiation Losses	
Non-uniform amplitude	0.14 db
Phase ripple	0.20
Mismatch in branch line	0.20
Total radiation losses	0.54
Conduction Losses	
In series feed line	1.00
In phasing and matching cables	0.15
In ground plane	0.30
Total conduction losses	1.45
Total losses	≅ 2.0

The losses in the series feed lines were obtained from the computer calculations for the phase and power at the outputs of the feeder lines. The loss in the phasing cables corresponds to a half-wavelength of RG-8/U (the average length of phasing cable) plus a quarter-wavelength of RG-11/U.

The ground losses were deduced from a set of measurements of the impedance of a dipole over a ground plane similar to that of the array. The measured impedances differed from

theoretical values by a quantity which could be accounted for by assuming a reflection coefficient of about 0.9, which corresponded to an estimated loss of about 0.3 db.

The peak directivity of the antenna was calculated to be 35.6 db for the broadside beam. The gain for this beam is therefore 33.6 db. The gain of the antenna is referred to its input point and therefore does not account for the losses that occur in the line connecting it to a transmitter or a receiver.

D. Radiation Pattern and Gain Measurements

The radiation patterns and the gain of the principal array have been measured for several beam directions in the N-S plane. These patterns were measured by flying an aircraft, equipped with a 38.25-Mcps oscillator and a suitable broad-beam antenna, at constant altitude in a S-N direction over the El Campo antenna site. The aircraft was tracked by a modified AN/SCR-584 radar, and the power received by the array was recorded as a function of radar elevation angle. The gain measurements were carried out by rapidly switching the receiver from the array antenna to a reference dipole antenna.

To measure the radiation patterns and gains with the accuracy corresponding to the usual far-field criterion, a flight altitude of 240,000 feet is required for the broadside beam. This requirement could not be met since the flying equipment available for the purpose permitted a maximum altitude of only 40,000 feet. The patterns and gains measured at this altitude differ appreciably from their far-field counterparts, but still provide a useful means of ascertaining the behavior of the antenna. The radiation patterns and gains expected at this altitude are discussed in Sec. II-D-1.

1. Radiation Patterns and Gains in the Fresnel Region

For the present purpose, the radiation patterns and gain of the array can be identified as those of a uniformly illuminated aperture with a progressive phase variation in its N-S direction. The directivity $G(\Theta, R)$ at a distance R from this aperture is given by

$$\frac{G(\Theta, R)}{G(\Theta_o, \infty)} = X[C(v_2) - C(v_1)]^2 + X[S(v_2) - S(v_1)]^2 \quad , \tag{48}$$

where C and S are the Fresnel cosine and sine integrals, respectively, and

$$v_2 = \frac{1}{2\sqrt{X}} \left(\frac{2uX}{\pi} + 1\right) \quad ,$$

$$v_1 = \frac{1}{2\sqrt{X}} \left(\frac{2uX}{\pi} - 1\right) \quad ,$$

$$u = \frac{2\pi L}{\lambda} (\sin\Theta - \sin\Theta_o) \quad ,$$

$$X = \frac{R}{(2L^2 \cos^2\Theta)/\lambda} \quad ,$$

L = aperture length in the N-S direction,

Θ_o = direction of peak of the beam,

$G(\Theta_o, \infty)$ = far-field peak directivity .

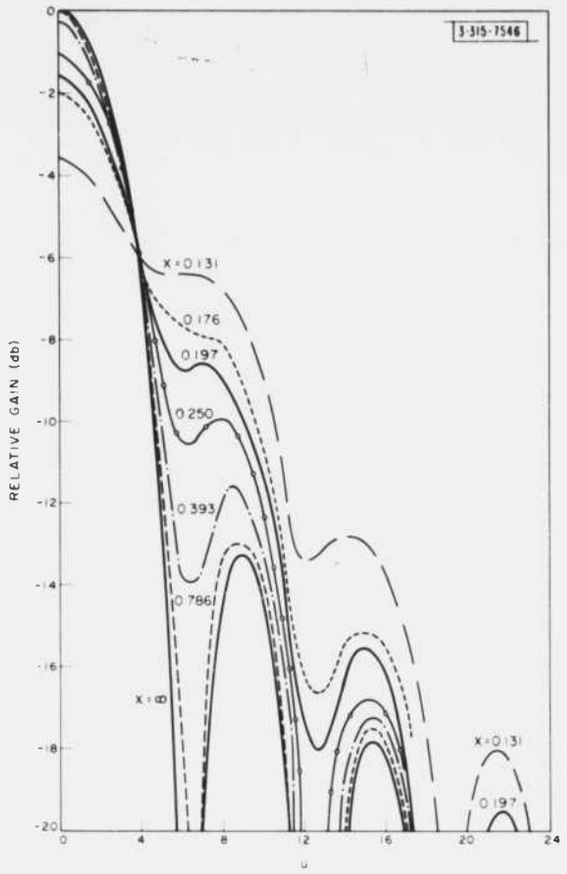

Fig. 27. Radiatian patterns in Fresnel regian.

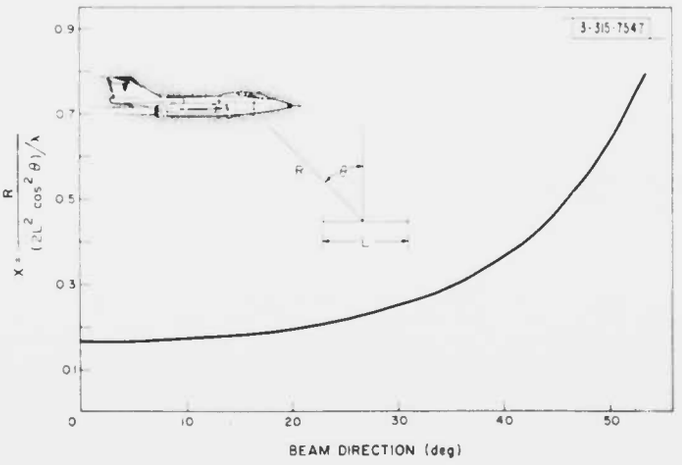

Fig. 28. Ratio af measuring distance ta far-field distance vs beam direction (altitude = 40,000 feet).

Graphs of this expression as a function of the variable u, with X as a parameter, are given in Fig. 27. With large apertures that have small beamwidths, the parameter X may be considered constant over a range of angles encompassing the beam and the first few side lobes. The graphs are then fairly accurate representations of the patterns in the Fresnel region. For a fixed flight altitude, the measuring range increases with scan angles; therefore, the ratio of the measuring range to far-field distance (X) also increases with scan angle. The correspondence between the parameter X and the beam direction is expressed by the curve of Fig. 28 for a flight altitude of 40,000 feet. The Fresnel patterns are almost identical to their far-field counterparts for beam directions far off broadside. As the beam direction approaches broadside, the principal effects of measurements in the Fresnel region are filling in of the nulls, higher side lobes, and larger beamwidths. The largest effect occurs in the broadside beam and corresponds to a beamwidth broadening of about 25 percent and an increase of 9 db in the first side lobes.

The peak directivity of the antenna in the Fresnel region is obtained by making $\theta = \theta_o$ in Eq. (48). The decrease of peak directivity is plotted as a function of beam direction for a constant flight altitude of 40,000 feet in Fig. 29. Maximum reduction occurs for the broadside beam and is about 2.2 db. At 52.5° – the lowest scan angle for which pattern measurements were made – the gain reduction is only 0.2 db.

2. Reference Antenna

The reference antenna used for gain measurements was a near-resonant half-wave dipole mounted parallel to ground, and polarized in an E-W direction. The dipole cross section was 1.75 inches, its length 140 inches, and its height above ground the same as that of the array element (4 feet, 9 inches). For this set of parameters, the dipole base impedance is real and approximately 50 ohms. To improve the ground reflectivity, wire mesh (chicken wire) was laid over an area 50 feet square, centered under the dipole.

The reference antenna radiation patterns are identical to those of the array element, because both the reference and element dipoles are parallel and located the same distance above ground. These patterns have been reported in Fig. 24.

The peak directivity of the reference dipole is equal to

$$\frac{480\, K^2 [1 - \cos(\pi L/\lambda)]^2 \sin^2(2\pi h/\lambda)}{R \sin^2(\pi L/\lambda)} , \qquad (49)$$

where L is the reference dipole length, h is its height above ground, R is its radiation resistance in ohms, and K is a nondimensional constant function of the dipole effective height which itself is a function of the dipole cross section. For the dipole parameters given, the values of K and R obtained from King[11] are, respectively, 1.08 and 52.0 ohms. Insertion of these values into Eq. (49), together with the values of the other parameters, yields a peak directivity of 6.72 or 8.26 db. It is interesting to note that this is equal to the peak directivity of an infinitely thin half-wave dipole mounted the same height above ground.[12]

The gain of the reference antenna is obtained by reducing its peak directivity by the losses inherent in the antenna. The principal source of losses occurs in the ground plane and was estimated from the data obtained by measuring the feed point impedance of dipoles of different lengths located above this ground plane. Comparison of the measured values with theoretical values yielded an average ground reflection coefficient of about 0.9. The corresponding ground loss is about 0.55 db, yielding a reference dipole gain of 7.7 db when fed with a lossless cable.

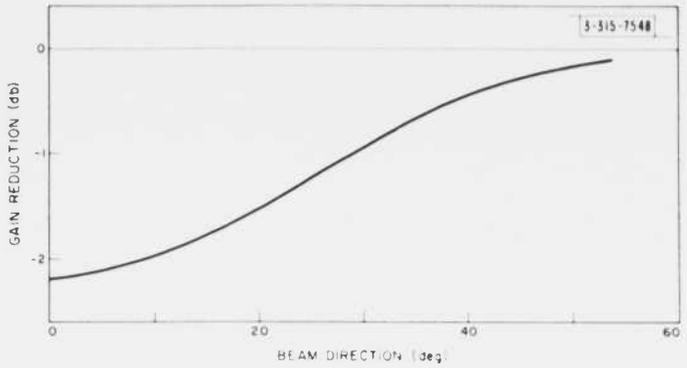

Fig. 29. Gain reductian at measurement distance vs beam direction.

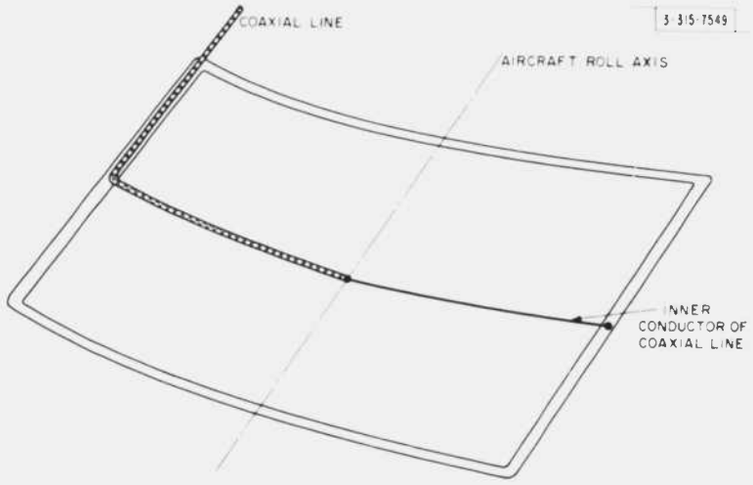

Fig. 30. Outline of feed line in aircraft radome.

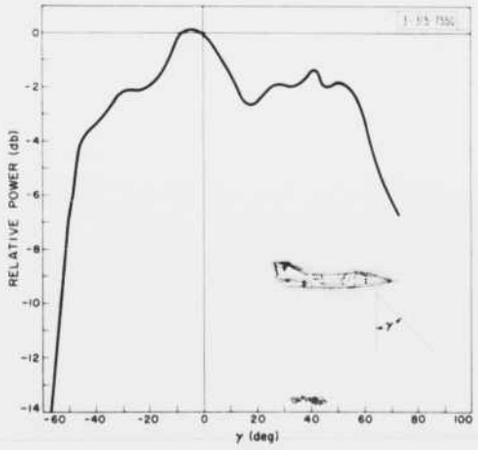

Fig. 31. Aircraft antenna pattern in pitch plane.

3. Airborne Antenna

A 38.25-Mcps antenna, polarized parallel to the pitch axis, was installed in an aircraft. The radiation pattern of this antenna in the pitch plane had to be as broad as possible. These requirements were met by exciting a cavity located under the fuselage and occupied by a radar antenna. The cavity, covered by a radome, is about 0.1λ deep and its perimeter is about 1λ. It was excited by running a feed line along the middle of the radome and parallel to the pitch axis of the plane (Fig. 30). The feed line was fed from its middle point, thereby providing an asymmetrical excitation of the orthogonal mode in the cavity; hence, no cross-polarized component was radiated in directions contained in the pitch plane. In other directions, there was a cross-polarized component of appreciable amplitude because of the large width of the cavity; however, since this component existed out of the measurement plane, it did not affect the results. The radiation resistance of this antenna was low, resulting in an efficiency estimated to be on the order of a few percent.

The pitch plane pattern of the antenna was measured by flying the aircraft in a S-N direction over the reference antenna described in the preceding section. The received power is then proportional to the product of the aircraft and reference antenna directivities, divided by the square of the distance between these two antennas. The aircraft antenna pattern deduced from these measurements is shown in Fig. 31.

4. Measurement Results

The far-field radiation patterns presented in Fig. 32(a-e) were obtained from power measurements received as the aircraft flew in an approximate N-S direction over the antenna site. The actual flight path was in a direction slightly west of true north, so that the aircraft could follow a radio beacon radial which crosses the peak of the beam in the meridian plane. The direction of the radial was between 4° and 5° west of north, depending on the beam elevation. By flying this radial, it was possible for the aircraft to pass repeatedly within a sector bounded by directions corresponding to about the −1-db points of the E-W radiation pattern. The original plan called for a true N-S flight path, with the ground tracking station keeping the aircraft on this path with verbal instructions. On most passes, the aircraft had a ground speed that approached 500 miles/hour. The SCR-584 radar was capable of manually tracking the aircraft at a maximum range of about 28 miles when the radar was operating well. The automatic tracking took over at a point 16.5 miles south of the antenna, allowing a maximum of two minutes before the main beam of the N-S radiation pattern was reached and a minimum of 25 seconds, depending on scan angle. The corrections made during manual tracking were inaccurate; those made during automatic tracking were too late. Fortunately, the radio beacon was available almost due north of the site. This permitted the aircraft to make its approach from as far as 35 miles south of the site (limited by an ADIZ zone), and to make necessary corrections by homing in on the required radial even before acquisition by the tracking radar. After acquisition, the recorder was switched on, and the received power was recorded as a function of aircraft elevation angle. The azimuth angle of the plane as it crossed the peak of the beam was also noted. The pattern was recorded over five to six passes for each direction of the array antenna beam. Differences in the main beam and in the side-lobe levels were observed between the patterns measured on each of these passes, probably because the path of the aircraft varied about ±3° when it crossed the peak of the beam. However, when identical passes were made, very good repeatability was obtained.

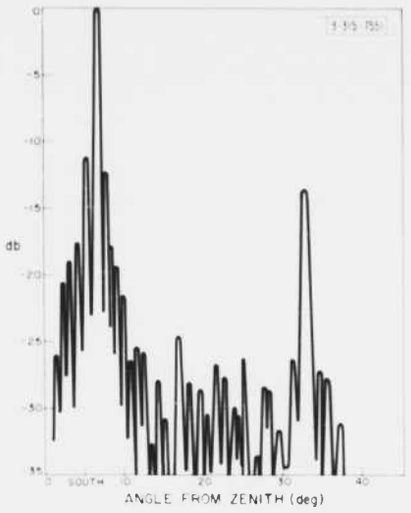

(a) Beom direction, 7.5°.

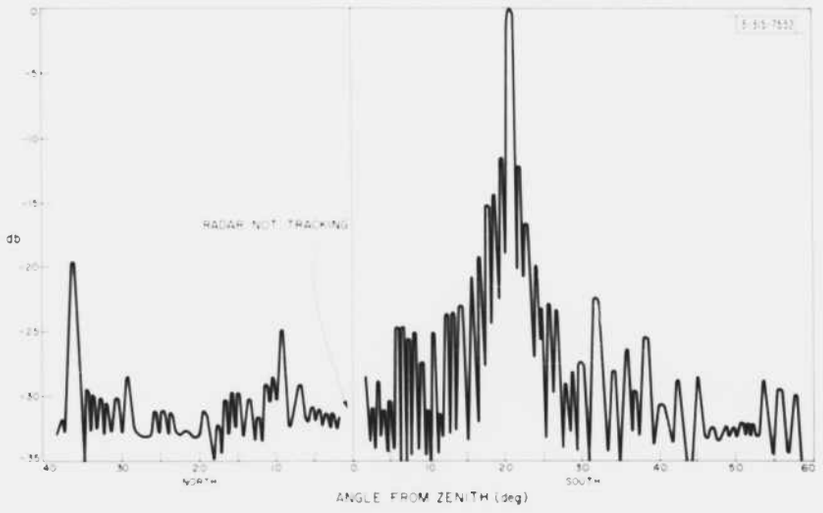

(b) Beam direction, 22°.

Figs. 32(a-e). Radiatian patterns in the N-S plane.

(c) Beam direction, 32°.

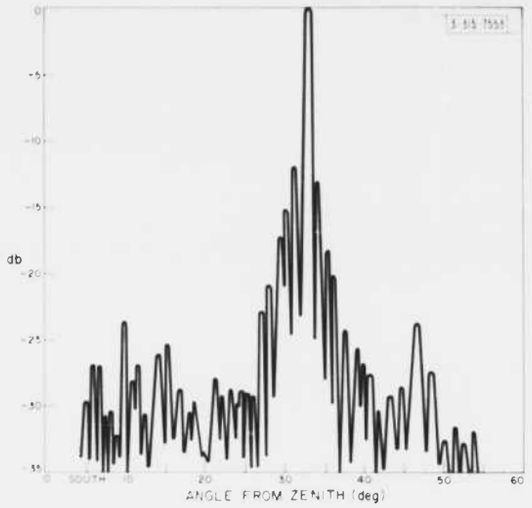

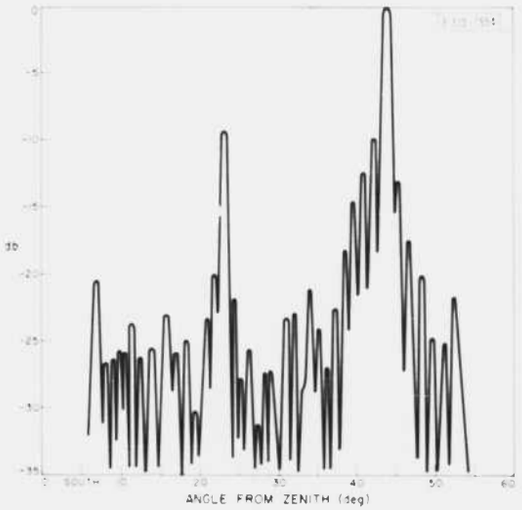

(d) Beam direction, 45°.

(e) Beam direction, 52.5°.

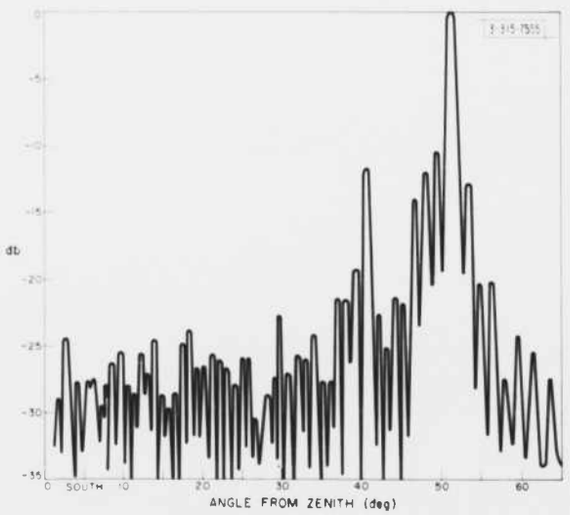

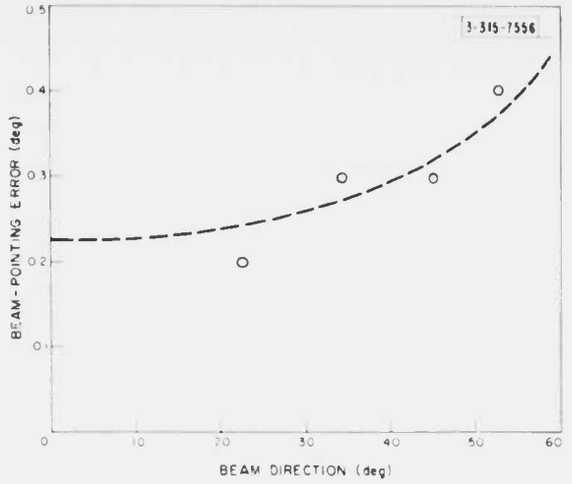

Fig. 33. Beam-pointing error as a function of beam directian.

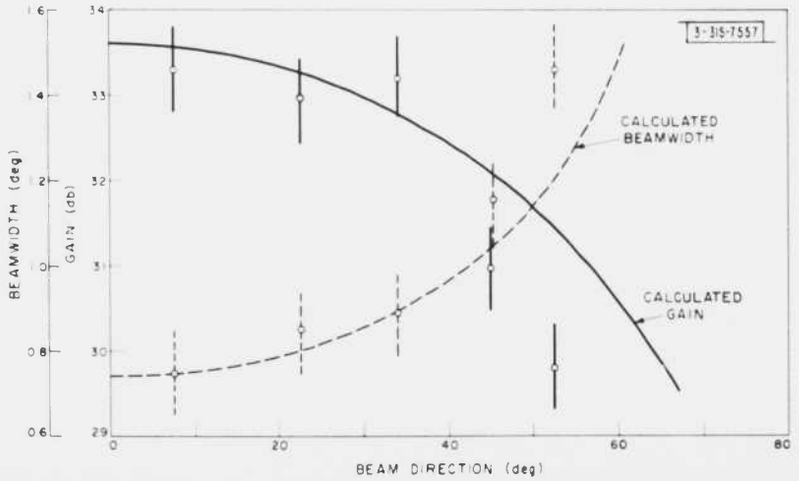

Fig. 34. Measured and colculated gains and beamwidths as a functian of beam direction.

The received power as a function of aircraft elevation was converted to antenna patterns by removing the contributions of the aircraft antenna directivity and range variation. This yielded Fresnel region patterns which were then converted to far-field patterns by applying a correction equal to the difference between the corresponding patterns of the ideal array. The angular scale on the measured patterns bears a small parallax error amounting to about 1.68°. This parallax results from the different location of the tracking radar and of the array center. As mentioned above, the measurement plane was not exactly the meridian plane, but a vertical plane that made an angle of 4° to 5° with the meridian. The differences between the patterns in these two planes are negligible for most of the recorded range of angles; they are noticeable only for the far-out side lobes. For instance, as the angle in the measuring plane departs from the beam axis, the aircraft moves out of the meridian plane. Therefore, side lobes are measured which are smaller than their value in the meridian plane. The angle between the radius vector to the aircraft and the meridian plane reaches 6° when the departure from the beam axis in the measuring plane is about 45°. At this angle from the beam axis in the meridian plane, the side lobes should be about 3 db larger than the corresponding measured ones.

The measured patterns are in fairly good agreement with predictions. In particular, location of spurious beams and their levels agree well with the calculated values.

The measured beam directions (averaged over all passes and corrected for parallax) deviate from their calculated values by a few tenths of a degree in the northern direction. This deviation, plotted in Fig. 33, increases with scan angle and could be accounted for by assuming a wave velocity in the series feed lines which is about 0.4 percent smaller than its calculated value. Results obtained from radio astronomy measurements and from sun radar experiments seem to confirm the pointing error.

The measurement of the half-power beamwidths from the antenna pattern recordings was inaccurate. The combination of radar tracking error and sticky synchro-gear trains resulted in large beamwidth variations of patterns recorded in nearly identical passes. A system was devised which eliminated the tracking. As the plane approached the peak of the beam, the recorder chart-drive input was switched from synchro to constant speed. This provided a measure of the 3-db beamwidth vs time which could be translated to elevation angles, since the chart rate and the aircraft speed and elevation as it crossed the beam were known. Beamwidths measured in this manner are plotted in Fig. 34 as a function of scan angle. For comparison, the predicted values are also plotted. The accuracy of the beamwidth measurements is about ±10 percent.

Gain measurements were carried out by switching the receiver to the reference antenna for a moment, after the passage of the aircraft through the beam. The effects of a change in the aircraft attitude were thus minimized. The measured gain as a function of scan angle is also plotted in Fig. 34, together with the predicted values. Good agreement exists for scan angles from broadside to about 30°. The measurements at 45° and 52.5° deviate appreciably from the theoretical values. One possible effect responsible for this behavior is the element mismatch. It is noticed, in the radiation patterns, that the spurious beam which results from this mismatch is formed in a direction close to the main beam for the larger scan angle; therefore, the assumption made earlier that there is little interference between the two no longer holds.

Section II-B-4 pointed out that neglect to correct the phase error, due to the nonuniform wave velocity in the series feed lines, would result in gain loss and pattern asymmetry. This was ascertained by taking patterns without phase correction, and a typical pattern taken with the beam

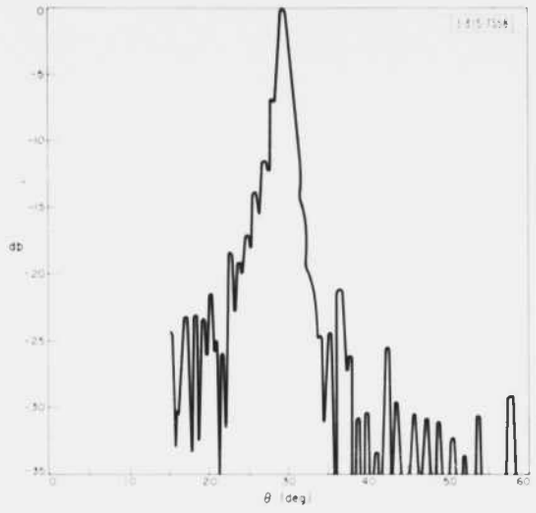

Fig. 35. Radiation pattern in the N-S plane for o beam direction of 30° when the phase error is not corrected.

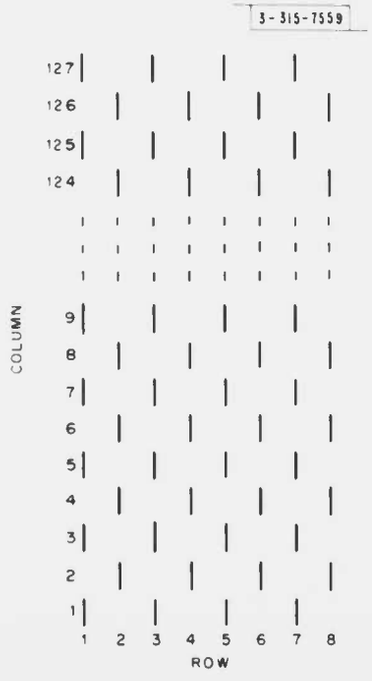

Fig. 36. Arrangement of dipoles in orthogonol orroy ontenna.

scanned to 30° south is presented in Fig. 35. Similar results were obtained, whatever the beam direction. The gain reduction due to the phase error was estimated at about 1.5 db. The antenna was used in this condition for about nine months as part of a system for measurement of radar reflections from the sun.

III. ORTHOGONAL ARRAY

The design specifications for the orthogonal array were essentially the same as those of the principal array, except that high-power handling capability was not required and larger feed losses could be tolerated since a gain somewhat smaller (about 2 db) than that of the principal array was acceptable. Also, to reduce the cost of this array, the specifications with respect to the scan angle at which a grating lobe is formed were relaxed to permit halving the number of elements needed. The detailed design of this array and supervision of its construction was carried out by Lincoln Laboratory members.

A. General Description

The orthogonal array consists of 512 elements perpendicular to the dipoles of the principal array. Its over-all size is equal to that of the principal array. The elements of this array are disposed in a triangular lattice; in column one there is a dipole in rows 1, 3, 5, 7; in column two there is a dipole in rows 2, 4, 6, 8. All odd columns are the same as column one; the even columns are the same as column 2. A single trough line, running along row 5, collects the signals received by the dipoles through a series of couplers separated 13-3/4 feet, as in the feeder lines for the principal array. A 4:1 power divider collects the signals from a column of dipoles and delivers them to the coupler in that column. The couplers and power dividers are designed to provide uniform illumination for the orthogonal array. The elements are similar to, and are located immediately above, the elements of the principal array. There is no matching stub, or transformer, and the dipole length is not adjustable. Dipole length was chosen to yield good impedance characteristics over the operating range of beam positions.

The orthogonal array is "phased" by inserting appropriate lengths of cables between the couplers and the input to the power dividers in a manner similar to that of the principal array.

B. Detailed Description

1. Element Spacing

The orthogonal array was built over the principal array to reduce its cost by making use of the same land surface and some of the same supports. The number of elements required for this array was halved by doubling the spacing between the dipoles along the rows. The appearance of a grating lobe at the lower scan angles of interest was not considered detrimental for this antenna. A triangular lattice arrangement was obtained by staggering the dipoles in every other row (Fig. 36). This array exhibits grating lobes for scan angles located in a region much larger than that of the principal array, as is evidenced by comparing Fig. 37 to Fig. 3. The range of scan angles characterized by the absence of a grating lobe is smallest in the azimuth plane $\varphi = \pm 45°$, for which this lobe appears at a scan angle of 19° only. In other planes the corresponding angle is larger; it is maximum (36.3°) in the two principal planes. The amplitude of the grating lobe with respect to the peak of the beam is determined by the element pattern which is discussed in Sec. III-C. The locus of scan angles for which the grating lobe is 13 db below the main beam is plotted in Fig. 37 for this particular element pattern.

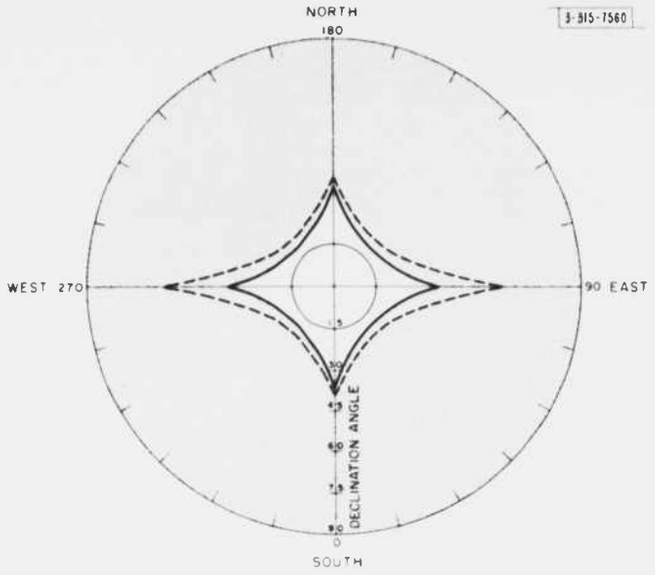

Fig. 37. Solid angle over which the beam of the orthogonal array can be sconned without the formatian af a grating lobe (outside shaded orea). Dashed curve is the locus of beom angles for which o –13-db grating lobe is formed.

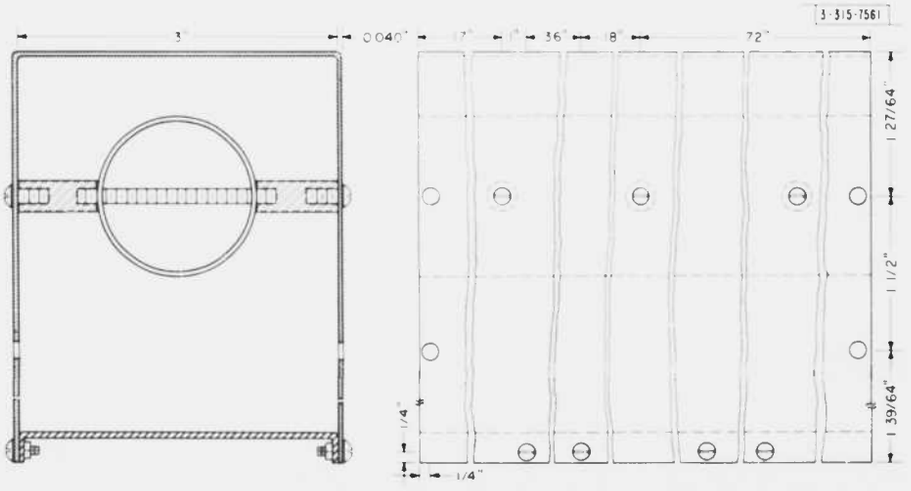

Fig. 38. Trough line for orthogonol arroy.

2. Feeder Line

The primary feeder line of the orthogonal array is also a trough line. Its cross section is smaller than that of the principal array feeder line, and both inner and outer conductors are made of aluminum. The larger conductor loss that results is acceptable in view of the smaller gain requirement for the antenna. The geometry of this line is shown in Fig. 38. Its normally open side was closed with an aluminum cover at installation. This cover may prevent some of the corrosion, insect, dampness, and grass problems associated with the open trough line used in the principal array. The section of the line which contains the coupler is 22 inches long. This length was chosen to permit the use of standard 12-foot lengths of aluminum tubing and sheet metal for the section of the line connecting successive couplers.

The output of each coupler (total 128) is fed into a 4:1 power divider. A schematic of this divider, made of 50-ohm coaxial transmission line, is shown in Fig. 39. The lengths of lines designated outputs 1, 2, 3, and 4 are unequal in order to direct the beam 3.35° to the west. The feed point impedance of the dipoles depends on scan angle and upon their location inside the array. When fed with 50-ohm cables, the average reflected wave at the feed point corresponds to a VSWR of about 1.5:1.0. At the center of the first tee, from each pair of dipoles, the impedance is therefore about 25 ohms. This impedance is transformed to about 100 ohms by a 50-ohm characteristic impedance transmission line which is an odd number of quarter-wavelengths long. At the input tee, the resulting input impedance is therefore about 50 ohms. The cables which are used to adjust the phase of the current are inserted at this point.

The coupler design for the orthogonal array is shown in Fig. 40. The capacitive coupling is varied by changing the length and the diameter of the center electrode. This design is somewhat easier to assemble and less expensive than that used on the principal array. Since this array is used for receiving only, no power handling problem exists.

3. Coupling Coefficient Calculation

The attenuation of the orthogonal array trough line, calculated from the estimated value of the principal array trough lines, is 3.4 db. When this value is inserted in the coupling coefficient computation program described in Sec. II-B-3, the results expressed in Fig. 41 are obtained. Approximation of the required coupling values to ±0.5 db yields the design values expressed by the dotted curve in this figure. Couplers of seventeen different coupling values are required to realize this line.

4. Power and Phase at Feeder Line Outputs

The calculated power at the output of each coupler as a function of the coupler number is given in Fig. 42. For comparison, the measured values are also given. The calculated and measured values of the phase differential between the phase of the voltage appearing at the output of a given coupler and the preceding one are plotted as a function of coupler number in Fig. 43. The power and phase differential measurements show appreciably larger variations than expected. A similar behavior was observed in the principal array feeder lines. The factors that may account for the discrepancies, however, are not all the same for both feeder lines. For the principal array feeder lines, the salient factors were listed in Sec. II-B-4. For the orthogonal array feeder line, these factors are:

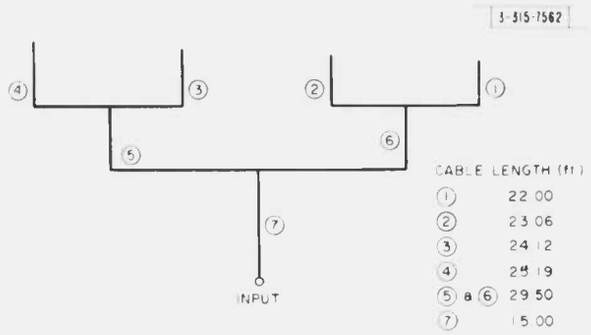

Fig. 39. Pawer divider.

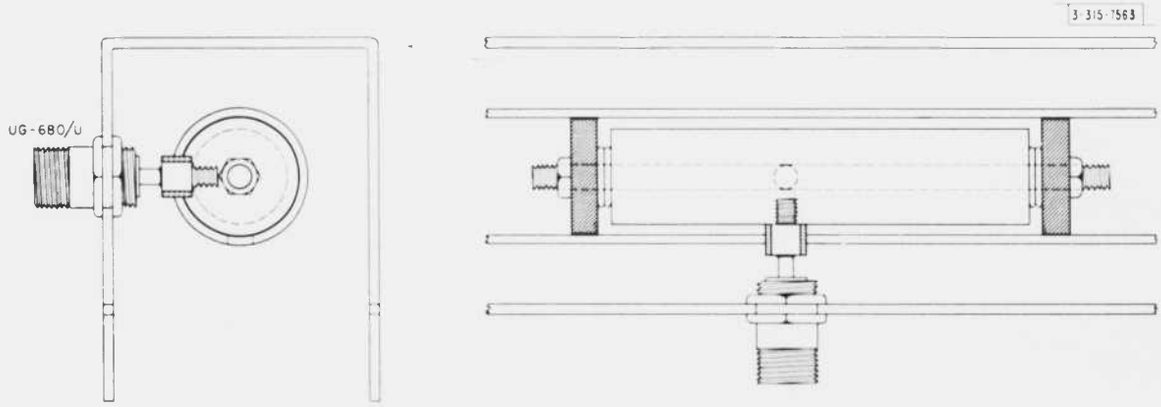

Fig. 40. Couplers for arthogonal array feeder line.

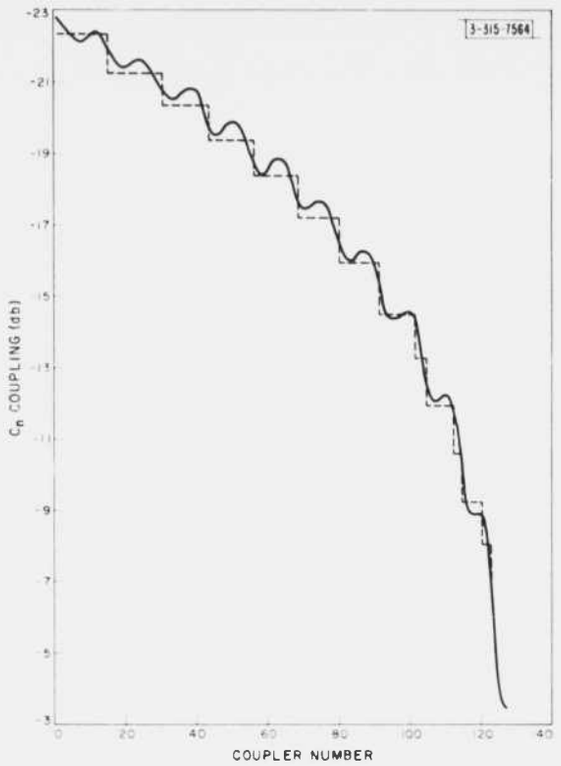

Fig. 41. Coupling coefficient as a function of coupler number (orthogonal array).

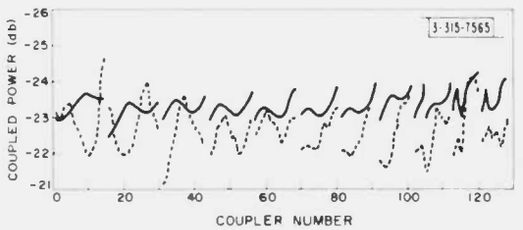

Fig. 42. Calculated (solid line) and measured (dashed line) power at feeder line outputs (orthogonal array).

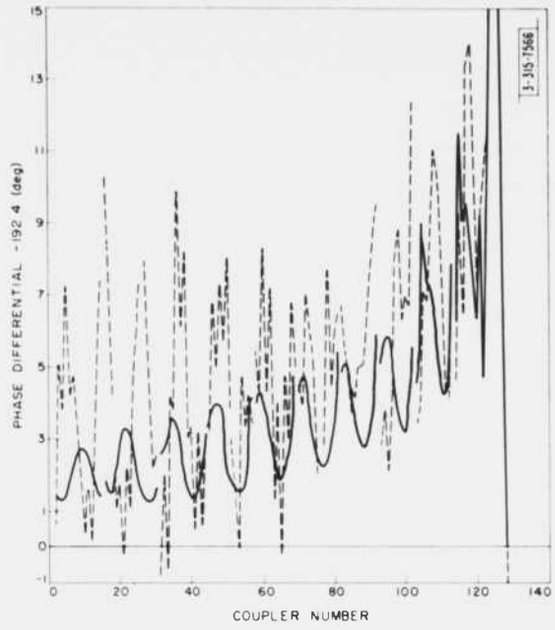

Fig. 43. Calculated and measured phase differential of orthogonal array feeder line.

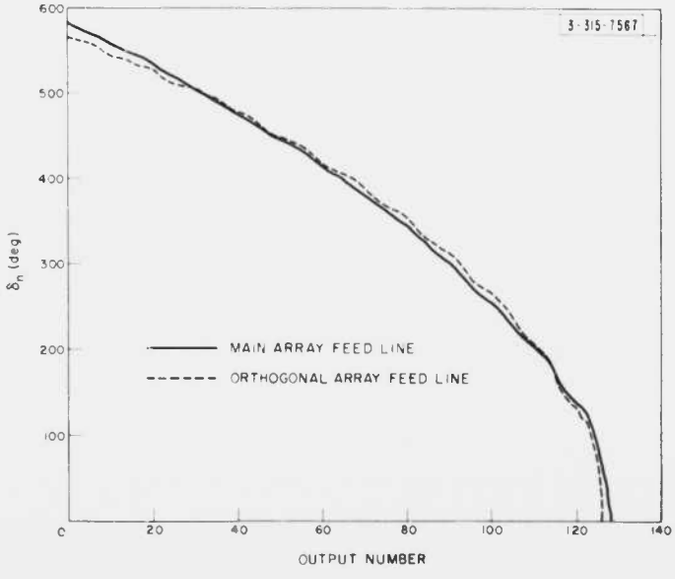

Fig. 44. Phase increase of loaded line as a function of coupler number as compared with unloaded line values.

(a) The open side of the 50-ohm trough line was covered to eliminate the troubles experienced with an open line. This resulted in an estimated line characteristic impedance about 5 ohms less than the 50-ohm value used in the calculation.

(b) The line attenuation constant used for the calculation corresponds to a 3.4-db attenuation loss for the unloaded line. A value of 2.4 db was measured.

(c) Reflections at the supports for the center conductor were neglected in the calculation.

The phase of the voltage at the output of the couplers, as a function of coupler location along the line, varies nonlinearly in a manner similar to that of the principal array feeder lines. This phase is larger than its value in the absence of the couplers by a quantity which is plotted in Fig. 44 as a function of coupler number. The corresponding quantity for the principal array feeder lines, also plotted on this figure, is so close to the former that the wave velocity in the two types of lines may be assumed to be the same, and therefore the same correction is required in their branch lines.

It should be noted, however, that the phase differential measurements indicate mean values which lie close to the predicted ones for the principal array feeder lines (see Fig. 14), but are about 1° larger for the orthogonal array feeder line (Fig. 43). This behavior would indicate a wave velocity that is slower in the orthogonal array feeder line than in the principal array lines, with the consequence that the cross-polarized array beam would be directed about 0.25° higher than that of the principal array when the two arrays are phased similarly. However, measurements of phase differentials for both arrays were not carried out with exactly the same measuring equipment, and the relative accuracy between the two is not known to better than 1.0°. More accurate measurements are therefore required to substantiate the previous conclusion.

5. VSWR at Feeder Line Input

The calculated input VSWR with 50-ohm loads in place of the elements is about 1.15:1.0. With the elements connected to the feeder line, the input VSWR should not change appreciably for all scan angles except at, and close to, broadside. For a broadside beam, the reflected wave from the mismatch of each element reaches the input in phase, causing a larger VSWR. The input VSWR should then be equal to the average value of that existing in the branch lines, or about 1.5:1.0.

6. Measured VSWR and Relative Power of Forward Wave in Branch Lines

The radiation impedance of the dipoles of the orthogonal array is about 50 ohms. Because of the larger spacing between elements of this array, the variation of this impedance with scan angle is smaller than that of the principal array. The length of the dipoles is such that a suitable match exists for the entire range of scan angles from 0° to 52.5° from broadside. This length, as found by trial and error, is 134 inches. The height above ground of the orthogonal dipoles is about 4 inches more than that of the dipoles of the principal array. The VSWR in the branch lines was measured over the section of the array between rows 42 to 51 inclusive. This measurement was carried out for scan angles of 0°, 15°, 30°, 45°, and 52.5°. The currents in elements 36 to 56 were phased to point the beam in the required direction; we considered this sufficient to insure operation similar to that obtained when the entire array was excited to produce a beam in that direction. The results plotted in Fig. 45 are for the elements located in rows 4 and 5. Measurements taken on the other rows yielded results similar to these two rows, except for scan angles of 45° and

52.5° for which the average value of the VSWR for all eight rows is about 1.65, a value somewhat smaller than that obtained for rows 4 and 5.

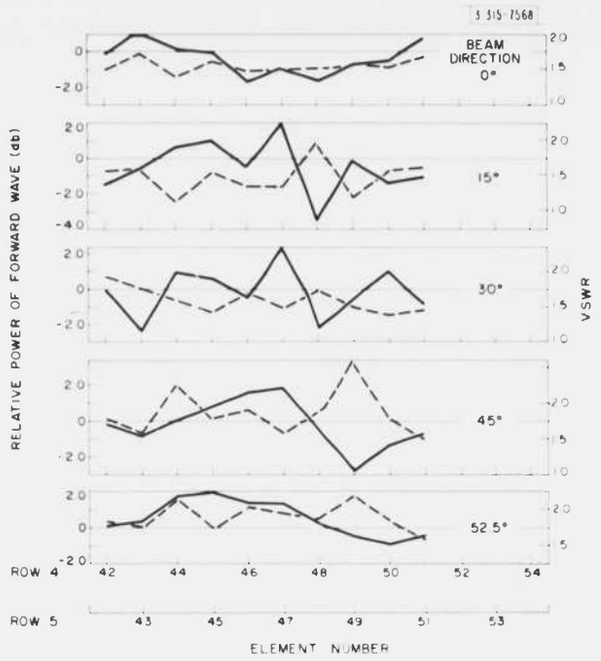

Fig. 45. Relative power of farward wave (salid line) and VSWR (dashed line) in a few successive branch lines af arthagonal array.

The relative power of the forward wave in the branch lines of this part of the array was also measured and is also plotted in Fig. 45.

7. Cross Coupling Between the Principal and Orthogonal Arrays

Eaeh dipole of the orthogonal array is mounted so that the eross-polarized dipole sharing the same post lies in its neutral plane. This minimizes the coupling between these two dipoles. Furthermore, eoupling between eross-polarized dipoles located on different posts is very small for dipoles located well inside the array; it is a little larger for the dipoles loeated on the edge rows. This behavior is readily understood if one observes that the current indueed by a dipole of the prineipal array is almost eanceled by that of another dipole of the prineipal array whieh is symmetrically located with respect to the axis of the orthogonal dipole. The degree of eaneellation depends upon the difference of the current amplitude in these two symmetrieal dipoles.

Measurement of eross eoupling between the two antennas yielded a value of −70 db. When this measurement was made, the beam deelination was 22° south. It should be noted that the eross eoupling depends on the sean angle and that it should be small for most sean angles, exeept for the broadside direction where it should be eonsiderably higher beeause the element phasing is then suitable for reinforeement. The eross eoupling at this angle is expeeted to be on the order of −25 to −30 db.

C. Calculated Directivity Patterns and Estimated Gain

1. Directivity Patterns of Uniformly Excited Array

Under the same provisions as for the principal array, the directivity function for this array is

$$D(\theta, \varphi) = \frac{480 \sin^2(2\pi h \cos\theta/\lambda) \cos^2(\frac{\pi}{2} \sin\theta \cos\varphi)}{M_1 M_2 R(\theta_o, \varphi_o)(1 - \sin^2\theta \cos^2\varphi)}$$

$$\times \frac{4 \sin^2 \frac{M_1 v_1}{2} \sin^2 \frac{M_2 v_2}{2} \cos^2\left(\frac{v_2 - 2v_1}{4}\right)}{\sin^2 v_1 \sin^2 \frac{v_2}{2}} \quad , \tag{50}$$

where d_1 is the spacing between rows, d_2 is the spacing between elements in a row, M_1 is the number of rows, M_2 is the number of dipoles per row, and

$$v_1 = \frac{2\pi d_1}{\lambda} (\sin\theta \sin\varphi - \sin\theta_o \sin\varphi_o) \tag{51}$$

$$v_2 = \frac{2\pi d_2}{\lambda} (\sin\theta \cos\varphi - \sin\theta_o \cos\varphi_o) \quad . \tag{52}$$

For beam directions located in the meridian plane, the directivity in the plane ($\varphi = \varphi_o = 0$) is

$$D(\theta, 0) = \frac{480 M_1 \sin^2(2\pi h \cos\theta/\lambda) \cos^2(\frac{\pi}{2} \sin\theta)}{M_2 R(\theta_o, 0) \cos^2\theta} \frac{\sin^2 M_2 \frac{\pi d_2}{\lambda} (\sin\theta - \sin\theta_o)}{4 \sin^2 \frac{\pi d_2}{2\lambda} (\sin\theta - \sin\theta_o)} \quad . \tag{53}$$

The spacing between elements of a row of the orthogonal array is twice that of the principal array ($d_2 = 2d$), the number of dipoles per row is half ($M_2 = N_2/2$), and $M_1 = N_1$. Substitution of these values in Eq. (53) yields

$$D(\theta, 0) = \left[\frac{240 N_1 N_2 \sin^2(2\pi h \cos\theta/\lambda) \cos^2(\frac{\pi}{2} \sin\theta)}{R(\theta_o, 0) \cos^2\theta}\right]$$

$$\times \left[\frac{\sin N_2 \frac{\pi d}{\lambda} (\sin\theta - \sin\theta_o)}{N_2 \sin \frac{\pi d}{\lambda} (\sin\theta - \sin\theta_o)}\right]^2 \quad . \tag{54}$$

The normalized array factor in the meridian plane (second factor) is identical to that of the principal array [Eq. (36)] but it is quite different in other planes. For instance, it was shown in preceding sections that the orthogonal array exhibits a first grating lobe for scan angles in the meridian plane larger than 36°, whereas this behavior occurs for scan angles larger than 60° for the principal array. However, the first grating lobe of the orthogonal array points in directions nearly perpendicular to the meridian plane, and therefore does not modify the pattern in that plane.

The element factor of the orthogonal array is almost identical to that of the principal array rotated 90°. A slight difference should exist because they are located at slightly different heights above ground.

a. Calculation of Phasing Cable Length

Figure 44 showed that the calculated phase characteristics of the orthogonal array feeder line are very nearly the same as those of the principal array feeder lines. Since the spacing between couplers in the two arrays is the same, the lengths of the phasing cables as calculated for the principal array also apply to the orthogonal array. However, as mentioned earlier, measurements of the phase differentials between successive couplers for the two types of feeder lines indicated a slower wave velocity in the orthogonal type, hence, the orthogonal array beam may point about 0.25° above that of the principal array. Systematic errors may account for the difference of wave velocity in the two lines, and more accurate measurements would be required to ascertain the relative position of the two cross-polarized beams.

b. Peak Directivity of Orthogonal Array

The peak directivity of the broadside beam of the orthogonal array antenna is obtained from Eq. (53) with $\Theta = \Theta_o = 0$. The result is

$$D(0, 0) = \frac{480\ M_1 M_2 \sin^2(2\pi h/\lambda)}{R(0, 0)} \quad . \tag{55}$$

The element broadside radiation resistance $R(0, 0)$ was approximated by replacing it by the radiation resistance of a half-wavelength infinitely-thin dipole surrounded by four similar, equally fed, equispaced dipoles in echelon (5-element array). These four echelon dipoles correspond to the four nearest dipoles surrounding an element inside the orthogonal array. The radiation resistance thus obtained is about 53 ohms or about half that of the principal array. As the number of dipoles $M_1 M_2$ in this array is also half the number in the principal array, the gain is the same. This is no surprise since each array covers the same area and there are no grating lobes when the beam points in the broadside direction.

The peak directivity of the orthogonal antenna, as a function of the scan angle, depends upon the radiation resistance of its elements. The element radiation resistance is an unknown function of this scan angle. Calculation of the radiation impedance as a function of scan angle in the meridian plane for the 5-element array referred to above indicated only a slight variation of its resistive part. Impedance measurements performed on a representative group of elements of the orthogonal array confirmed this behavior. With nearly constant element radiation resistance, the gain variation as a function of scan angle in the meridian plane becomes proportional to the element directivity in this plane. This latter is given by the $\varphi = 90°$ curve in Fig. 24.

2. Effects of Deviations from Uniform Excitation on Directivity Patterns

The orthogonal array excitation function differs from the ideal uniform function: the principal deviations are nearly identical to those of the principal array, except for the smaller amplitude ripple and the absence of an excess of power in the last part of the feeder line. The effects on the directivity patterns caused by the phase ripple and the element mismatch, therefore, are the same as those for the principal array; the effects of the amplitude ripple are too small to be of concern.

3. Estimated Gain

The peak directivity of the broadside beam of the orthogonal array is equal to that of the principal array, and therefore equal to 35.6 db. The radiation losses resulting from nonuniform excitation are:

Nonuniform amplitude	0.02 db
Phase ripple	0.20
Mismatch in branch lines	0.20
Total radiation losses	0.42

The estimated conduction losses are:

In the series feed line	1.60
In the power dividers and phasing cables (about 75 feet of RG-8/U)	0.90
In the ground plane	0.30
Total conduction losses	2.80

The total loss in the orthogonal array, therefore, amounts to about 3.2 db; the loss incurred in the transmission line which joins the receiver to the antenna input is not included. The broadside gain of the orthogonal antenna array is $35.6 - 3.2 = 32.4$ db when it is excited with a lossless transmission line.

The radiation pattern and gain of the orthogonal antenna array have not been measured directly. However, results obtained in experiments on radar reflections from the sun suggest a performance close to predictions.

IV. CONCLUSION

A 38.25-Mcps antenna consisting of two orthogonally polarized planar arrays, each with a gain larger than 30 db, has been constructed and is now operating satisfactorily as part of a solar radar system. The Fresnel region directivity patterns of one of these arrays have been measured and good agreement with theoretical predictions has been obtained.

ACKNOWLEDGMENTS

The design of the antenna was initiated by Dr. S. Rabinowitz, farmerly of Lincoln Laboratory, and now with Columbia University.

The authors wish to express their oppreciation to the Flight Test Program Branch of Wright Patterson Air Force Base for cooperation in securing the aircraft for the directivity pattern measurements. They are also indebted ta many members of Lincoln Laborotary, in particular to Mr. W. C. Danforth and Miss M. H. Malone who programmed the IBM 7090 computer, and to Messrs. L. J. Ricardi and to J. H. Chishalm and members of Group 33, for their helpful criticisms and suggestions.

REFERENCES

1. F. J. Kerr, "On the Possibility of Obtaining Radar Echoes from the Sun ond Planets," Proc. IRE 40, 660-666 (June 1952).
2. W. G. Abel, et al., "Rador Reflections from the Sun at Very High Frequencies," J. Geophys. Research 66, 4303-4307 (December 1961).
3. E. D. Sharp, "A Triangular Arrangement of Planar-Array Elements That Reduces the Number Needed," Trans. IRE PGAP, AP-9, 126-129 (Morch 1961).
4. E. L. Ginzton, Microwave Measurements (McGraw-Hill, New York, 1957), pp. 469-470.
5. P. S. Carter, Jr., "Mutual Impedance Effects in Large Beam Scanning Arrays," Trans. IRE, PGAP AP-8, 276 (May 1960).
6. S. Edelberg ond A. A. Oliner, "Mutual Coupling Effects in Large Antenna Arrays II: Compensation Effects," Trans. IRE PGAP AP-8, 360-367 (July 1960).
7. W. P. R. King, The Theory of Linear Antennas (Harvard University Press, Cambridge, 1956), Chap. III.
8. J. L. Allen, et al., "Phased Array Radar Studies," Technical Report No. 228 [U], Lincoln Laboratary, M. I. T. (12 August 1960), Part 3, ASTIA 249470, H-335.
9. _____, "Phased Array Radar Studies," Technical Report No. 236 [U], Lincoln Laboratory, M. I. T. (13 November 1961), ASTIA 271724.
10. H. A. Wheeler, "The Radiatian Resistance of an Antenna in an Infinite Array or Waveguide," Prac. IRE 36, 478-487 (April 1948).
11. W. P. R. King, op. cit., Secs. 7.3, 9.4, and 14.5.
12. John D. Krauss, Antennas (McGraw-Hill, New York, 1950), pp. 296.

For convenience in ordering copies of Lincoln Laboratary reports cited in this document, each reference is followed by its ASTIA number. In addition, Unclassified (released) reports have also been assigned Hayden serials (designoted H-), indicating that they are obtoinable, at cost, as micrafilm or photoprint copies from the Microreproduction Service, Hayden Memorial Library, M. I. T., Cambridge 39, Massachusetts.